OLIO
A7
6
963
.25
p. 2

DISSERTATION

FALL VELOCITY OF ARTIFICIAL POROUS PARTICLES

Submitted by

Komain Unhanand

In partial fulfillment of the requirements

for the Degree of Doctor of Philosophy

Colorado State University

Fort Collins, Colorado

June 1963

LIBRARIES
COLORADO STATE UNIVERSITY
FORT COLLINS, COLORADO

CER 63 KU 25

DISSERTATION

FALL VELOCITY OF ARTIFICIAL POROUS PARTICLES

Submitted by

Komain Unhanand

In partial fulfillment of the requirements

for the Degree of Doctor of Philosophy

Colorado State University

Fort Collins, Colorado

June 1963

ABSTRACT OF DISSERTATION

FALL VELOCITY OF ARTIFICIAL POROUS PARTICLES

The objective of this research is to study the fall velocity of artificial porous particles. It is expected that this study will lead to further research concerning transport of flocules or porous particles in fluids.

Two types of porous particles having two different porosities were made by cementing bearing balls together. Then another set of particles identical to the two types above were made with all pores sealed. These particles were released individually in six fluids of different viscosities and the fall velocity was found by photographic means.

The drag coefficients of these particles were computed. The experimental results show that there is negligible difference in the drag coefficient of the porous and sealed particles of Type I (porosity ≈ 0.175), except at Reynolds number greater than 10^4. For Type II particles (porosity ≈ 0.380), the porous particles show appreciably higher values of the drag coefficient than the sealed ones, except at Reynolds number smaller than 30.

The characteristics of the drag coefficient curves seem to agree satisfactorily with the theoretical analysis. This theoretical analysis included considerations of the pressure drag, shear drag, and shear resistance along the flow passage due to flow through the particle.

Komain Unhanand
Civil Engineering Department
Colorado State University
June 1963

LIBRARIES
COLORADO STATE UNIVERSITY
FORT COLLINS, COLORADO

COLORADO STATE UNIVERSITY

June 1963

IT IS RECOMMENDED THAT THE DISSERTATION PREPARED BY

Komain Unhanand

ENTITLED FALL VELOCITY OF ARTIFICIAL POROUS PARTICLES

be accepted as fulfilling this part of the requirement for the degree of Doctor of Philosophy

Committee on Graduate Work

Major Professor

Head of Department

Examination Satisfactory

Chairman

Permission to publish this dissertation or any part of it must be obtained from the Dean of the Graduate School.

ACKNOWLEDGEMENTS

The writer wishes to express his sincere appreciation and gratitude to Dr. A. R. Chamberlain, the writer's major professor, for his valuable comments and suggestions, encouragement and unfailing support which make this research possible.

The generous assistance and valuable suggestions of Professor E. F. Schulz in the experimental work are hereby acknowledged.

The writer expresses his warm gratitude to the other members of the committee, Dr. I. S. Dunn, Dr. A. T. Corey, and Dr. R. H. Niemann, for their valuable comments, suggestions and their review of the dissertation and to Professor M. E. Bender, Head of the Civil Engineering Department.

TABLE OF CONTENTS

TABLE OF CONTENTS--Continued

FIGURES

TABLES

SYMBOLS AND DIMENSIONS

Symbol	Definition	Dimension
A	Maximum projected area of the particle	L^2
A_H	Non-solid portion of the external surface	L^2
A_S	Solid portion of the external surface	L^2
C_D	Drag coefficient	---
D	Total drag in Stoke's equation $D = 6\pi \mu R U_\infty$	F
D_P	Pressure drag	F
D_S	Shear drag	F
d	Diameter of bearing balls	L
d_n	Nominal diameter of particle	L
e	Base (2.7183) of natural system of logarithms	---
f	Frequency of stroboscope	rpm
$\overline{F}$	Body force vector = $F_x i + F_y j + F_z k$	F
F_x, F_y, F_z	Components of body force	F
g	Acceleration due to gravity	L/T^2
K	Correction factor	---
k	Mean height of asperity on particle surface	L
L	Length of flow passage in pores of particle	L
N	Number of images between the two images measured	---
n	Porosity	---
p	Intensity of pressure	F/L^2
R	Radius	L
Re	Reynolds number	---
r, θ, ϕ	Spherical coordinates, and $r^2 = x^2 + y^2 + z^2$ in Cartesian coordinates	L, degree

SYMBOLS AND DIMENSIONS--Continued

Symbol	Definitions	Dimension
R_p	Mean radius of pore passage	L
S	Shear resistance along pore surface	F
t	Time	T
U_∞	Free stream velocity	L/T
u,v,w	Velocity components	L/T
u',v',w'	Components of perturbation velocity	L/T
V_o	Terminal fall velocity	L/T
V_S	Volume of the solid portion of the porous particle	L^3
W_a	Weight of the porous particle in air	F
W_B	Bouyant weight of particle	F
ζ	Vorticity	---
μ	Dynamic viscosity	FT/L^2
ν	Kinematic viscosity	L^2/T
ρ	Mass density	FT^2/L^4
ρ_f	Mass density of fluid	FT^2/L^4
ρ_s	Mass density of liquid	FT^2/L^4
τ	Shearing unit stress	F/L^2
τ_C	Average shearing unit stress between the fluid and the sealed surface area over the holes	F/L^2
τ_H	$\frac{\text{Shear drag on the non-solid area}}{\text{Non-solid area}}$	F/L^2
τ_S	Average shearing unit stress between the fluid and the solid external surface of the particle	F/L^2
ψ	Stream function	---

CHAPTER I

INTRODUCTION

In applying theoretical methods for describing the movement of sediment and predicting the amount of sediment transport in streams, certain hydraulic properties of the sediment particles are required. The terminal fall velocity or settling velocity is salient among these sediment properties (12).

Many studies on the terminal fall velocity, both theoretical and experimental, have been conducted. The relationship of important properties influencing the fall velocity such as the shape factor has been discovered and represented in graphical as well as tabular forms. Most of these works were done for solid non-porous sediment particles. However, under certain circumstances, the sediment may be in the form of flocules and, therefore, it should not be treated in the same manner as solid particles in the analysis of its movement.

A flocule may be defined as a group or cluster of individual sediment particles, produced by floculation (or coagulation) (13). For this reason, the behavior of a flocule may not resemble that of a solid particle. Since the terminal fall velocity is required in the analysis of the transport of solid particles, it is logical that in an attempt to analyze the movement of a flocule or artificial porous particle the terminal fall velocity of the flocule would again be required.

The objective of the research reported herein is to study the characteristic fall velocity of artificial porous particles. The writer hopes that this study will create a starting point for further research in

the field of transport of sediment flocules or artificial and natural porous particles. In this study the terminal fall velocity of several artificial porous particles, made by cementing stainless bearing balls together in certain arrangements, was found.

CHAPTER II

REVIEW OF LITERATURE

Man has encountered the sedimentation problem since time immemorial. The problems became more serious when man started to utilize more water from streams to fulfill the increasing needs of irrigation, navigation, hydro-electricity, and municipal and domestic supply. One of the most serious problems is sedimentation in reservoirs, where in some cases, the sediments are in the form of flocules (13).

However, it was not until about the latter part of the seventeenth century, when a more modern science of sedimentation engineering began (5). But, unfortunately, comparatively little progress seems to have been made in the study of the transportation and deposition of sedimentary materials until after two decades of the twentieth century had passed. Beginning about 1920, there was a rapid increase in the number of studies concerning sediment movements. The most recent works on the subject includes those of E. W. Lane, H. Rouse, V. A. Vanoni, H. A. Einstein, L. G. Straub, and others.

In their analyses of sediment movement, an evaluation of some hydraulic properties of the sediment is required and the terminal fall velocity is one among them. Fall velocity has been found by dropping particles in various fluids and measuring the rate of fall by a stopwatch (12) or a photographic technique (6).

Theories describing the motion of particles falling freely in fluids have been derived by several scientists. Unfortunately, most theories are valid only for the solid particle having certain form and moving at a very slow speed or at low Reynolds number. No theoretical

analysis has been developed to describe the motion of the particle of the porous type. For this reason, a review on the theory of the motion of a solid sphere moving in fluids will be discussed in this chapter.

A. Drag Coefficient and Reynolds Number

In the perfect fluid theory, a submerged body moving steadily through an infinitely extended fluid at rest will experience no resistance to motion, i.e. that its drag is zero (D'Alembert's paradox) (4)(15).

The fluid viscosity produces two basic types of drag--shear drag, caused by tangential shear along the boundary, and pressure drag, caused by the distribution of pressure which is applied normal to the surface of the boundary.

When the Reynolds number is very small, the inertial effects caused by the movement of a body are completely secondary to those of viscous forces. At high Reynolds number the inertial forces predominate over the viscous stresses. Separation may occur and the low intensity of pressure in the wake leads to a resultant force which opposes the motion. Since the magnitude of this force varies with the shape of the body, the drag coefficient in the region of high Reynolds number is distinctly a function of shape.

Most problems of flow around submerged objects involve both shear drag and pressure drag. The general drag equation may be written as (10)

$$F_D = \frac{C_D A \rho_f V_o^2}{2} \qquad 2.1$$

where F_D = drag force,

C_D = dimensionless drag coefficient,

A = projected cross-sectional area,

ρ_f = density of the fluid,

V_o = terminal fall velocity of the moving particle.

Numerous experiments have been conducted to find the value of the drag coefficient for particles having various shapes. For all particles of any one shape, C_D will conform to a single curve of C_D vs Reynolds number, Re, for which Re expresses the relative effect of inertial and viscous forces (14). The C_D vs Re curves may be found in references (1), (2) and (9).

B. Sphere Moving in Fluids at a Very Slow Motion

G. G. Stokes (11) was the first to derive an analytical expression describing the motion of a sphere through viscous fluid for the case where the viscous forces are considerably greater than the inertial forces. In this case, the inertial terms are simply omitted from the equations of motion. The resulting solutions are valid only when the velocity of the sphere is very small, or when the Reynolds number is very small (i.e. $Re \ll 1$).

The Navier-Stokes equations for incompressible flow may be written as

$$\rho \frac{D\bar{w}}{Dt} = \bar{F} - \text{grad } p + \mu \nabla^2 \bar{w} \qquad 2.2$$

where,

$$\frac{D\bar{w}}{Dt} = \frac{\partial \bar{w}}{\partial t} + \frac{d\bar{w}}{dt}$$

$\bar{w} = i\,u + j\,v + k\,w$,

u,v,w are the three orthogonal components of fluid velocity,

p = pressure,

ρ = mass density,

μ = dynamic viscosity,

$\overline{F} = F_x i + F_y j + F_z k$ = body force.

If the inertial terms are neglected, eq. 2.2 becomes

$$\text{grad } p = \mu \nabla^2 \overline{w} \qquad 2.3$$

The equation of continuity, in the case of non-steady flow of a compressible fluid, may be expressed by

$$\frac{\partial \rho}{\partial t} + \text{div } (\rho \overline{w}) = 0 \qquad 2.4$$

In an incompressibe fluid, with ρ = constant, the equation of continuity assumes the simplified form

$$\text{div } \overline{w} = 0 \qquad 2.5$$

Stokes solved eqs. 2.3 and 2.5 and gave the solution for the case of parallel flow past a sphere of radius R , with center at the origin, and which is located in a parallel stream of uniform velocity U_∞ at great distance from the sphere in the direction along the x-axis. The following equations expressed the pressure and velocity components as obtained from the solution (Fig. 1) (11).

$$\left.\begin{aligned} u &= U_\infty \left[3/4 \frac{R\, x^2}{r^3} \left(\frac{R^2}{r^2} - 1 \right) - \frac{1}{4} \frac{R}{r} \left(3 + \frac{R^2}{r^2} \right) + 1 \right. \\ v &= U_\infty \frac{3}{4} \frac{R\, x\, y}{r^3} \left(\frac{R^2}{r^2} - 1 \right) \\ w &= U_\infty \frac{3}{4} \frac{R\, x\, z}{r^3} \left(\frac{R^2}{r^2} - 1 \right) \\ p - p_\infty &= - \frac{3}{2} \frac{\mu\, U_\infty\, Rx}{r^3} \end{aligned}\right\} \qquad 2.6$$

where $r^2 = x^2 + y^2 + z^2$

From eq. 2.6, the pressure on the surface becomes

$$p - p_\infty = - \frac{3}{2} \mu \frac{x}{R^2} U_\infty \qquad 2.6a$$

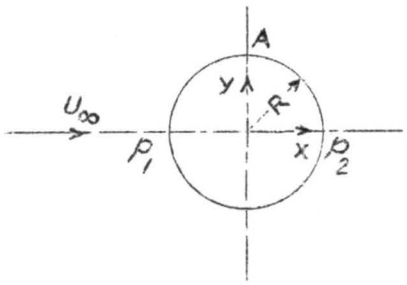

Fig. 1 A sphere in parallel uniform flow (11)

The maximum and minimum of pressure occur at points P_1 and P_2 respectively, their values being

$$p_{1,2} - p_\infty = \pm \frac{3}{2} \mu \frac{U_\infty}{R} \qquad 2.6b$$

The shearing stress distribution over the sphere can also be calculated from the above formulae. The maximum shear stress occurs at point A where $\tau = \frac{3}{2} \mu \frac{U_\infty}{R}$ and is equal to the pressure rise at p_2. The total drag, which is the sum of the pressure drag and shear drag, may be obtained by integrating the pressure distribution and the shear stress over the surface of the sphere.

$$\text{Total drag} = D = 6 \pi \mu R U_\infty \qquad 2.7$$

The above equation is known as Stokes equation for the drag of a sphere.

A comparison between Stokes' equation and experiment shows that it applies only to cases in which $Re < 1$.

C. Oseen's Improvement

C. W. Oseen (11), in 1910, improved Stokes' equation by taking into account partly the inertial terms in the Navier-Stokes' equations.

The velocity components are represented as the sum of a constant and a perturbation term.

$$u = U_\infty + u' \ , \quad v = v' \ , \quad w = w' \qquad 2.8$$

where u' , v' , and w' are the perturbation terms and hence small with respect to the free stream velocity U_∞ . It is to be noted that this is not true in the neighborhood of the sphere. By neglecting the second order terms such as $u' \frac{\partial u'}{\partial x}$, $u \frac{\partial v'}{\partial x}$, . . . which are small in comparison with the first order terms, we obtain the following equations of motion from Navier-Stokes equations:

$$\left.\begin{aligned} \rho U_\infty \frac{\partial u'}{\partial x} + \frac{\partial p}{\partial x} &= \mu \nabla^2 u' \\ \rho U_\infty \frac{\partial v'}{\partial x} + \frac{\partial p}{\partial y} &= \mu \nabla^2 v' \\ \rho U_\infty \frac{\partial w'}{\partial x} + \frac{\partial p}{\partial z} &= \mu \nabla^2 w' \\ \frac{\partial u'}{\partial x} + \frac{\partial v'}{\partial y} + \frac{\partial w'}{\partial z} &= 0 \end{aligned}\right\} \qquad 2.9$$

The boundary conditions are the same as for the Navier-Stokes equations, and the Oseen equations are linear as was the case with the Stokes equations. The pattern of streamlines (if plotted) is now no longer symmetrical about the axis of the sphere. The streamlines are closer together in front of the sphere which indicate higher velocity than in the former case.

The improved expression for the drag coefficient now becomes:

$$C_D = \frac{24}{Re}\left(1 + \frac{3}{16} Re\right) ; \quad Re = \frac{U_\infty (2R)}{\nu} \qquad 2.10$$

where C_D = drag coefficient,

Re = Reynolds number,

R = radius of the sphere,

ν = kinematic viscosity of the fluid,

whereas Stokes equation gives

$$C_D = \frac{24}{Re} \qquad 2.11$$

By comparison with the experimental results, it is evident that Oseen's equation is applicable up to $Re = 5$, approximately (11).

Goldstein (2), 1929, solved Oseen's equation in more detail and obtained

$$C_D = \frac{24}{Re}\left(1 + \frac{3}{16} Re - \frac{19}{1280} Re^2 + \frac{71}{20480} Re^3 \ldots\right) \qquad 2.12$$

which yields the value of drag coefficients closer to the experimental result than those of Oseen's equation.

Kawaguti (3) (1947) assumed special form of solution and satisfied an integrated form of the Navier-Stokes equations for the first and second order terms when expanded by Legendres polynomials. He obtained two solutions; one for $0 < Re < 10$, and the other for $10 < Re < 70$. These solutions did not justify the boundary-layer theory approximation in the region considered, and they give no information about the flow at the rear of the sphere at any Reynolds number.

A finite difference method was used by Thom (3) (1927) to solve Navier-Stokes equations for flow around cylinder at $Re = 10$, and this method was applied to flow around sphere at $Re = 20$ (1950) and cylinder at $Re = 40$ (1953) by Kawaguti. Allen and Southwell (3) solved the problem to flow around cylinders for $Re = 0, 1, 10, 100, 1000$ with satisfactory results, and Lister (3), in 1958, has used a modification of their method for sphreres at $Re = 0, 1, 10$, and 20.

D. Jenson's Solution of the Navier-Stokes Equations

V. G. Jenson (3), in 1959, interpreted the Navier-Stokes equations as vorticity transport equations and obtained some solutions by

using the method of relaxation. He divided the Navier-Stokes equations into two simultaneous second order equations by using the stream function (ψ) and introducing the vorticity (ζ) written in spherical polar coordinates

$$E^2 \psi = \zeta \, r \sin \theta \tag{2.13}$$

$$\frac{Re}{2}\left[\frac{\partial \psi}{\partial r}\frac{\partial}{\partial \theta}\left(\frac{\zeta}{r \sin \theta}\right) - \frac{\partial \psi}{\partial \theta}\frac{\partial}{\partial r}\left(\frac{\zeta}{r \sin \theta}\right)\right] \sin \theta = E^2 (\zeta \, r \sin \theta) \tag{2.14}$$

where $$E^2 = \frac{\partial^2}{\partial r^2} + \frac{\sin \theta}{r^2}\frac{\partial}{\partial \theta}\left(\frac{1}{\sin \theta}\frac{\partial}{\partial \theta}\right),$$

and r, θ = spherical coordinates,

Re = Reynolds number.

Then he made all quantities dimensionless by putting

$$r = \frac{r'}{R}, \quad \psi = \frac{\psi'}{U_\infty R^2}, \quad \zeta = \frac{\zeta' R}{U_\infty}, \quad Re = \frac{2 U_\infty R}{\nu}$$

where R = radius of sphere,

U_∞ = velocity of undisturbed stream,

ν = kinematic viscosity.

Because the stream function and vorticity are expected to vary most rapidly near the surface of sphere, it is necessary to have a fine lattice there and a coarser lattice at a greater distance. Jenson substituted the radial coordinate $r = e^z$ to accommodate for the gradation in lattice spacing and drew the lattice line at regular intervals of z. Equations 2.13 and 2.14 become

$$E^{2z} E^2 \psi = \zeta e^{3z} \sin \theta = 0 \tag{2.15}$$

$$\frac{Re}{2}\left[\frac{\partial \psi}{\partial z}\frac{\partial f}{\partial \theta} - \frac{\partial \psi}{\partial \theta}\frac{\partial f}{\partial z}\right] e^z \sin \theta - e^{2z} E^2 g = 0 \tag{2.16}$$

where $$e^{2z} E^2 = \frac{\partial^2}{\partial z^2} - \frac{\partial}{\partial z} + \sin\theta \frac{\partial}{\partial \theta}\left(\frac{1}{\sin\theta}\frac{\partial}{\partial \theta}\right),$$

and $$f = \frac{\zeta}{e^z \sin\theta},$$

$$g = \zeta e^z \sin\theta .$$

By considering lattice spacings in the z and θ-directions, eqs. 2.15 and 2.16 may be written in finite form, from which the solutions are obtained by applying the method of relaxation. Jenson presented his results for $Re = 5, 10, 20, 40$, in the form of stream function and vorticity distributions. Further results of pressure distributions, velocity distributions, and drag coefficient are calculated from them. These results are in good conformity with experimental work and show, at $Re = 5$, the near identical patterns of streamlines upstream and downstream of the sphere. At higher Reynolds numbers, separation begins to develop at the downstream side of the sphere, whereas the streamline pattern at the upstream side resembles that for irrotational flow.

The drag coefficient from Jenson's result are plotted in Fig. 2. The curve shows very good agreement with the experimental results. However, the solution for higher Reynolds numbers is needed to determine whether the good agreement will be maintained after the wake has been formed extensively behind the sphere.

E. Pressure Distribution Around a Moving Sphere

The pressure distribution around a sphere moving in fluids under different flow conditions is shown in Fig. 3 which is taken from (11). In the case of irrotational flow (or flow in invisid fluid) the pressure distribution is symmetrical on the upstream side and downstream side of

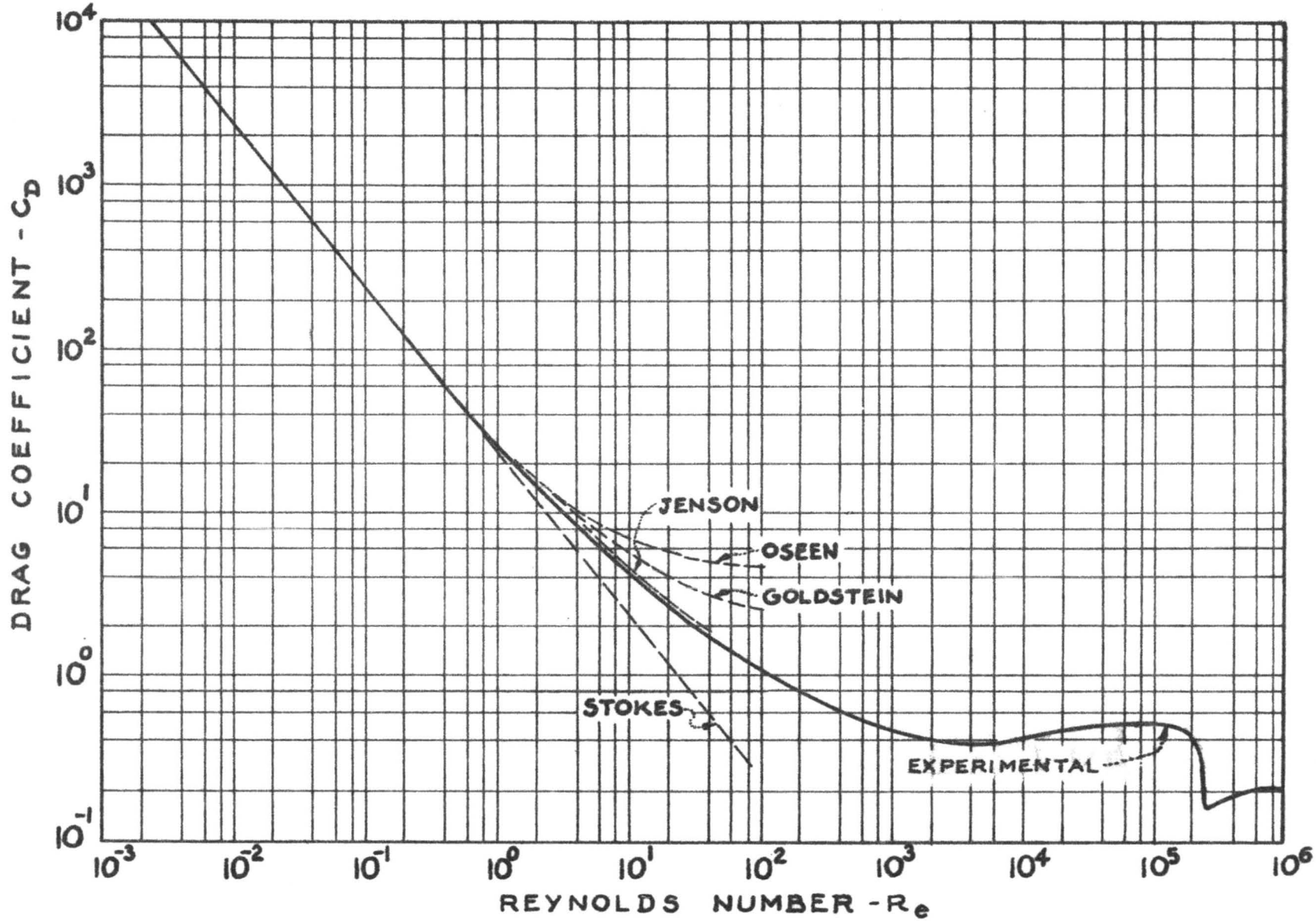

FIG. 2 – C_D VERSUS R_e CURVES FOR SMOOTH SPHERES

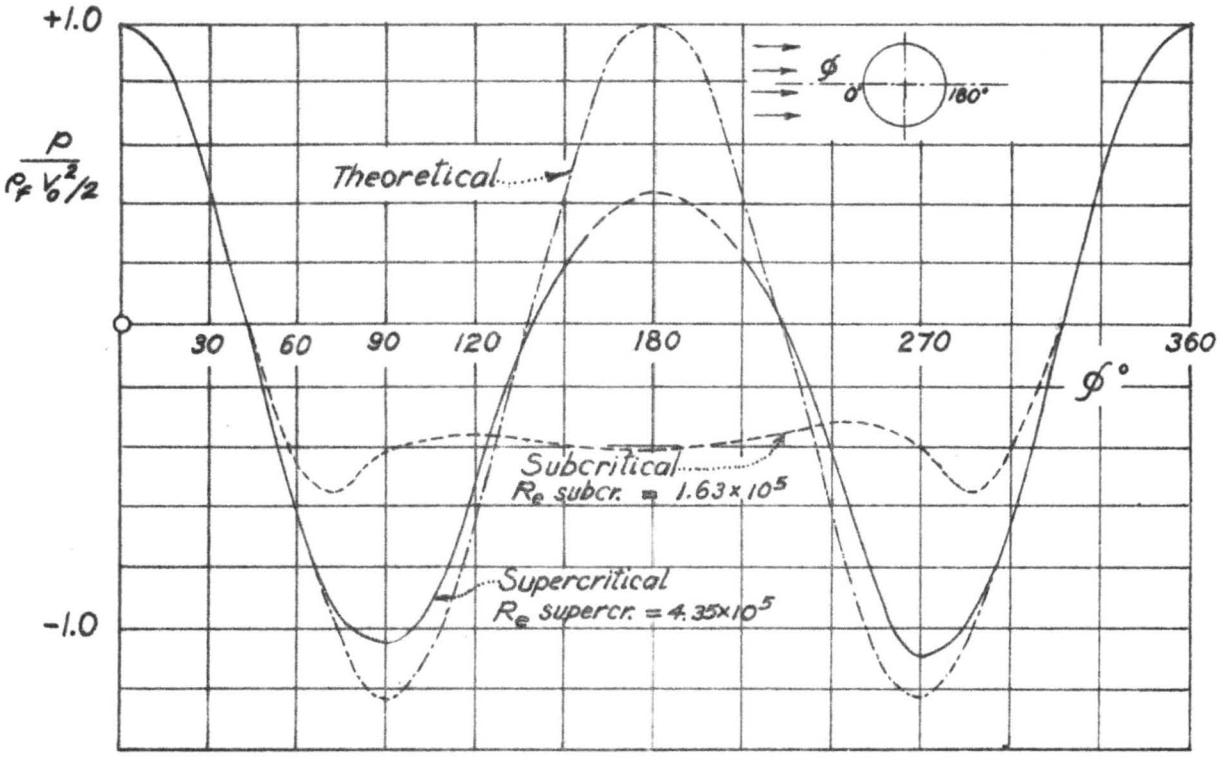

FIG. 3 - (11) PRESSURE DISTRIBUTION AROUND A SPHERE IN THE SUBCRITICAL AND SUPERCRITICAL RANGE OF REYNOLDS NUMBERS, AS MEASURED BY O. FLASCHSBART.

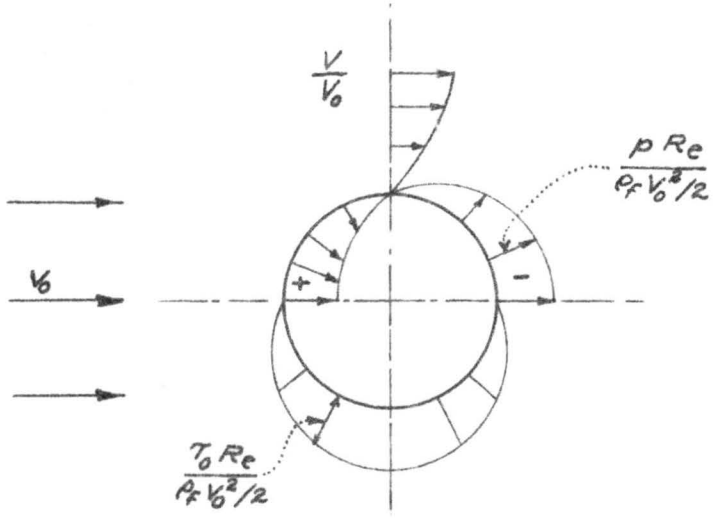

FIG. 4 - (1) DISTRIBUTION OF PRESSURE AND VELOCITY FOR FLOW AROUND A SPHERE AT $R_e < 0.5$

the object. As a result, the resultant pressure drag on the sphere moving in an invisid fluid is zero. Consequently, there is no drag on the upstream and downstream sides of the object, and no shear on the boundary of the object.

The other two curves in Fig. 3 show the measured pressures. Measurements indicate that the pressure distribution depends on the Reynolds number. The curve shows that the pressure distribution at high Reynolds numbers deviates less from the theoretical than at low Reynolds numbers. Figure 3 also shows that the smaller Reynolds numbers lie in the range of large drag coefficients, whereas the larger values lie in the range of small drag coefficients (i.e. at high Reynolds number the pressure distribution at the downstream side becomes positive which results in a decrease in total pressure drag).

Figure 4 (1) shows the pressure distribution in the case of a sphere moving in a fluid at a Reynolds number smaller than 0.5.

CHAPTER III

THEORETICAL ANALYSIS

The forces acting on falling particles are as follows:

1. the gravitational force acting on the particle,
2. the (tangential) shear force on the particle surface caused by fluid viscosity,
3. the pressure difference between the upstream and downstream side of the particle caused principally from inertial forces.
4. particle inertia (when it is in accelerating motion).

A. Basic Assumptions

The analysis of drag on falling particles are based on the assumptions that:

1. the fluid is of uniform density,
2. the fluid is of uniform viscosity,
3. the motion of the particle in the direction normal to the mean falling path (usually vertical) is negligible and involves no lateral acceleration of the particle,
4. the particle is not accelerating in the mean falling path.

B. Solid Particles versus Porous Particles

The general character of a porous particle in motion in a fluid, in comparison with that of a solid particle, may be described as follows:

1. There will be a smaller external solid surface subjected to shear stress from the fluid on a porous particle than on a solid one because of the holes on the surface of the porous particle.

2. Fluid flow may exist through the pores within a porous particle.

3. By the nature of porous particles, the external surface will possess some degree of roughness. It is impossible to make porous particles without having roughness on the surface.

C. Parameters Involved in the Analysis

By dimensional analysis, it may be shown for solid and porous particles with rough surface that

$$C_D = \Phi_1 \left(Re \ , \ \frac{k}{d_n} \ , \ n \ , \ \frac{d}{d_n} \right) \qquad 3.1$$

where C_D = drag coefficient,

Re = Reynolds number = $\frac{V_o \, d_n}{\nu}$,

ν = kinematic viscosity,

V_o = terminal fall velocity,

d_n = nominal diameter of the particle,

d = diameter of the bearing ball composing the particle,

k = mean height of asperity of the particle surface,

n = porosity of the particle.

For each type of particle having constant values for $\frac{k}{d_n}$, n , $\frac{d}{d_n}$, it is possible to write

$$C_D = \Phi_2 \ (Re) \ , \qquad 3.2$$

and a C_D and Re curve for the particle type may be drawn from the result of the experiments.

If $\frac{k}{d_n}$, and $\frac{d}{d_n}$ are kept constant, then

$$C_D = \Phi_3 \ (Re \ , \ n) \ , \qquad 3.3$$

and C_D vs Re curves showing the effect of n may be found.

D. Artificial Porous Particles

The porous particles used in this experiment are made from bearing balls cemented together in a certain pattern as fully described in Chapter IV. The system of forces on the particle when the particle is moving without acceleration in a fluid may be shown diagramatically in Fig. 5.

For equilibrium, $-W_B + D_P + D_S + S = 0$

or $$W_B = D_P + D_S + S \qquad 3.4$$

where W_B = bouyant weight of the particle in the fluid under consideration $= \frac{\pi d_n^3}{6} (\rho_s - \rho_f) g$,

D_P = pressure drag, in the same direction as W_B ,

D_S = shear drag on external surface, in the same direction as W_B ,

S = shear resistance along the surface of the pores, due to fluid flowing through the interior of the particle, in the same direction as W_B .

From drag coefficient eq. 2.1, the drag force is equal to the bouyant weight of the particle in the case of the particle descending in a fluid, then from eq. 3.4,

$$F_D = D_P + D_S + S \qquad 3.5$$

Substituting F_D in eq. 2.1,

$$D_P + D_S + S = C_D \frac{A \rho_f V_o^2}{2} ,$$

or $$C_D = \frac{2 (D_P + D_S + S)}{A \rho_f V_o^2} \qquad 3.6$$

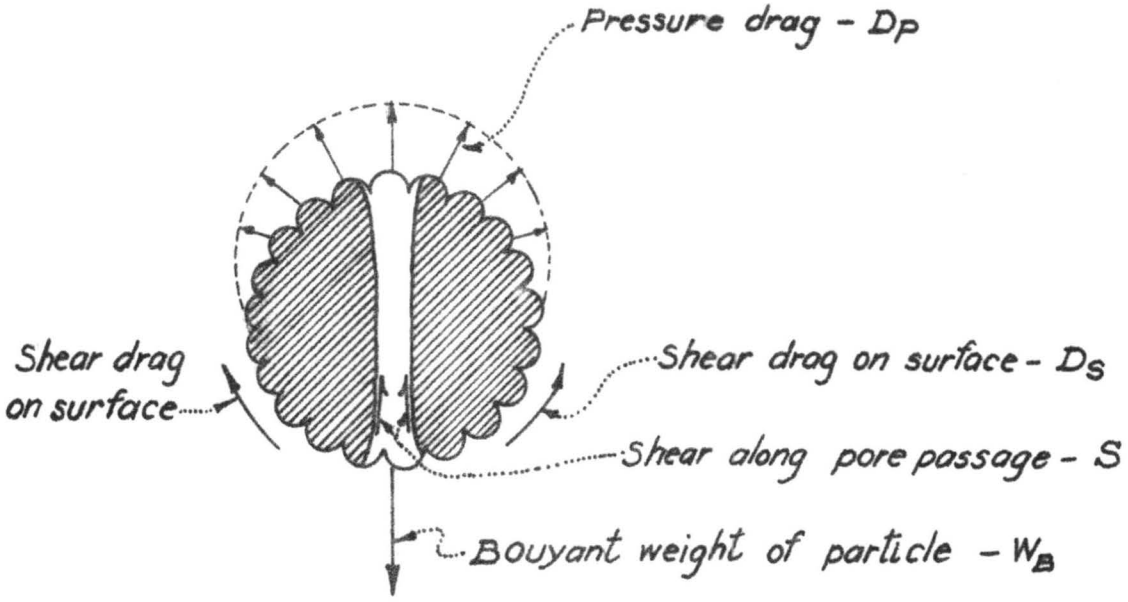

FIG. 5 - FORCES ON A POROUS PARTICLE

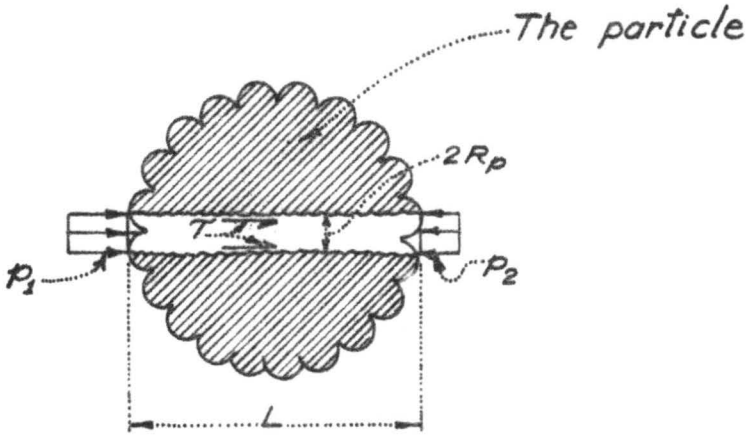

FIG. 6 - FORCES ON THE FLOW PASSAGE

E. General Shape of C_D vs Re Curves

By substituting W_B from eq. 3.4 into eq. 3.6, the drag coefficient may be expressed as

$$C_D = 2 \frac{W_B}{A \rho_f V_o^2} \qquad 3.7$$

An experiment to find the variation of C_D with Re may be conducted by dropping a single spherical particle in various kinds of fluids having different viscosity. In most cases the specific gravity of the fluids will vary from approximately 0.8 to 1.26, which indicates that the maximum variation in the mass density of the fluids will be in the neighborhood of 40-50 percent of its minimum values. But as for the fall velocity V_o, its value may vary as much as five times its minimum value. In short, it may be concluded that the variation of V_o is much greater than that of ρ_f.

Since only one spherical particle is employed and V_o is more significant than ρ_f, eq. 3.7 may be simplified as

$$C_D \sim \frac{1}{V_o^2} \qquad 3.8$$

Equation 3.8 indicates that, at high Re, C_D is small and it will increase as Re decreases (i.e. V_o decreases).

F. Drag Coefficient of Porous Particles in Comparison with Solid Ones

By considering two particles having similar shape (both are almost spherical) and external surface roughness except that one of them is porous and the other is solid, also by investigating each term in eq. 3.6, the comparison of drag coefficient of the two particles may be explained as follows:

1. Pressure drag D_P--Since Reynolds number is merely a ratio of the inertial force to the shear force, and the pressure drag results from the inertial force, it is expected that the pressure drag should be small at low Re , and should increase as Re increases.

The roughness on the surface should accelerate the formation of the separation zone behind the particle to occur at a relatively lower Reynolds number than it would if the roughness were not present. For this reason, one may expect that the pressure drag of the particle having rough surface should be greater than that of the particle having smooth surface at the same Re (in the range of $Re < 10^5$).

In conclusion, it may be written

$$\Delta D_P \sim Re \qquad 3.9$$

where ΔD_P = the difference in pressure drag D_P of a porous particle from that of the corresponding solid one.

2. Shear drag D_S--Shear drag for the porous particle may be expressed by

$$D_S = \tau_S A_S + \tau_H A_H \qquad 3.10$$

where τ_S = average shearing unit stress between the fluid and the solid external surface of the particle,

τ_H = effective average shearing unit stress resulted from the shear drag on the non-solid portion of the external surface, or $\tau_H = \dfrac{\text{shear drag on the non-solid area}}{\text{non-solid area}}$,

A_S = solid portion of the external surface,

A_H = non-solid portion of the external surface.

For a corresponding sealed particle, the similar expression may be written as

$$D_S = \tau_S A_S + \tau_C A_H \qquad 3.10$$

where τ_C = average shearing unit stress between the fluid and the sealed (or cemented) surface area over the holes.

Therefore the difference in shear drag between the two types of particles may be obtained by subtracting eq. 3.9 from eq. 3.10.

$$\Delta D_S = (\tau_C - \tau_H) A_H \qquad 3.11$$

As the viscosity increases, the Reynolds number is smaller, and the value of τ_H is approaching τ_C, which make possible to write

$$\Delta D_S \sim Re \qquad 3.12$$

3. Shear resistance along pore-surface S--This shear resistance does not exist in the case of solid particles since there is no flow through the interior of the particle. Therefore S itself represents the difference in shear resistance along the pore-surface between the porous and sealed particles.

Figure 6 shows forces acting on the flow passage formed by the pore space inside the porous particle.

Total shear resistance on pore surface = $2 \pi R_p \tau L = S$

Total pressure difference = $\pi R_p^2 (p_1 - p_2)$

For equilibrium, $\Sigma F_x = 0$, $S = \pi R_p^2 (p_1 - p_2)$ 3.13

Since $(p_1 - p_2)$ is directly proportional to D_P, then, from eqs. 3.13 and 3.9,

$$S \sim Re \qquad 3.14$$

From eq. 3.6, the difference in C_D between the porous and sealed particles may be expressed by

$$\Delta C_D \sim (\Delta D_P + \Delta D_S + S),$$

or

$$\Delta C_D \sim Re \qquad 3.15$$

According to eq. 3.15, the experimental result should show a very small difference in values of C_D of the porous and sealed particles at very small Reynolds numbers. The difference should be larger as the Reynolds number increases for the ranges of Re reported herein.

CHAPTER IV

EQUIPMENT AND PROCEDURE

The terminal fall velocity was determined from photographs of the particles taken during the fall with the aid of a stroboscope as the source of light.

The particles were dropped from a mechanical releaser attached at the top of the fall column. Also located at the top of the fall column was a stroboscope which was used as a source of light for photographing. A Polaroid camera was placed at a distance of approximately six feet from the center of the fall column. Successive images of the falling particles were obtained by the Polaroid camera because there was total darkness except at the intervals when the stroboscope illuminated the particle.

A scale graduated at five centimeter intervals was suspended at the longitudinal axis of the fall column, at the front quarter point, at the rear quarter point and photographs of the scale at each position were taken. A plastic scale was made by laying a clear plastic sheet over the photograph of the graduated scale at the center. The plastic overlay was marked directly from the corresponding distances on the photograph. Photographs of the graduated scale suspended at various other places were used for preparing a correction-factor curve to be applied to obtain the true distance of descent when the particle did not fall along the longitudinal axis of the fall column.

The time interval of flashes was obtained by setting the desired frequency on the stroboscope. The distance of fall during each flash

interval was found by the use of the prepared plastic scale overlay and the correction factor curve when the path of descent deviated from the center line of the column.

The terminal fall velocity was computed by the equation below.

$$\text{Fall velocity} = V_o = K_x \frac{\text{Distance from scale}}{N + 1} \times \frac{f}{60} \quad 4.1$$

where N = Number of images located between the two images measured.

f = Frequency of the stroboscope used in taking the picture of the particle, in rpm.

K = Correction factor as obtained from the prepared correction curve.

V_o = Terminal fall velocity (same unit as the distance from scale).

A. Equipment

The equipment consisted of a fall column, mechanical releaser, stroboscope, scale, camera, and film.

1. Description of each component of the equipment

(a) Fall column--The fall column, made of Plexiglass plastic 1/4-inch thick was 16 inches in inside diameter and ten feet long. The bottom was sealed with a 1/2 inch plastic sheet in an inclined position as shown in Fig. 7 so that the particle rolled down into the outlet plastic-hose which had a plastic cup attached at the end. A clamp was placed on the hose above the cup. The upper surface of the bottom sheet was covered with 1/4-inch thick sponge-sheet to act as a cushion. Furthermore, a circular screen made of cotton fabric sewn on a brass ring was lowered from the top of the column to a position about two to three inches above the bottom

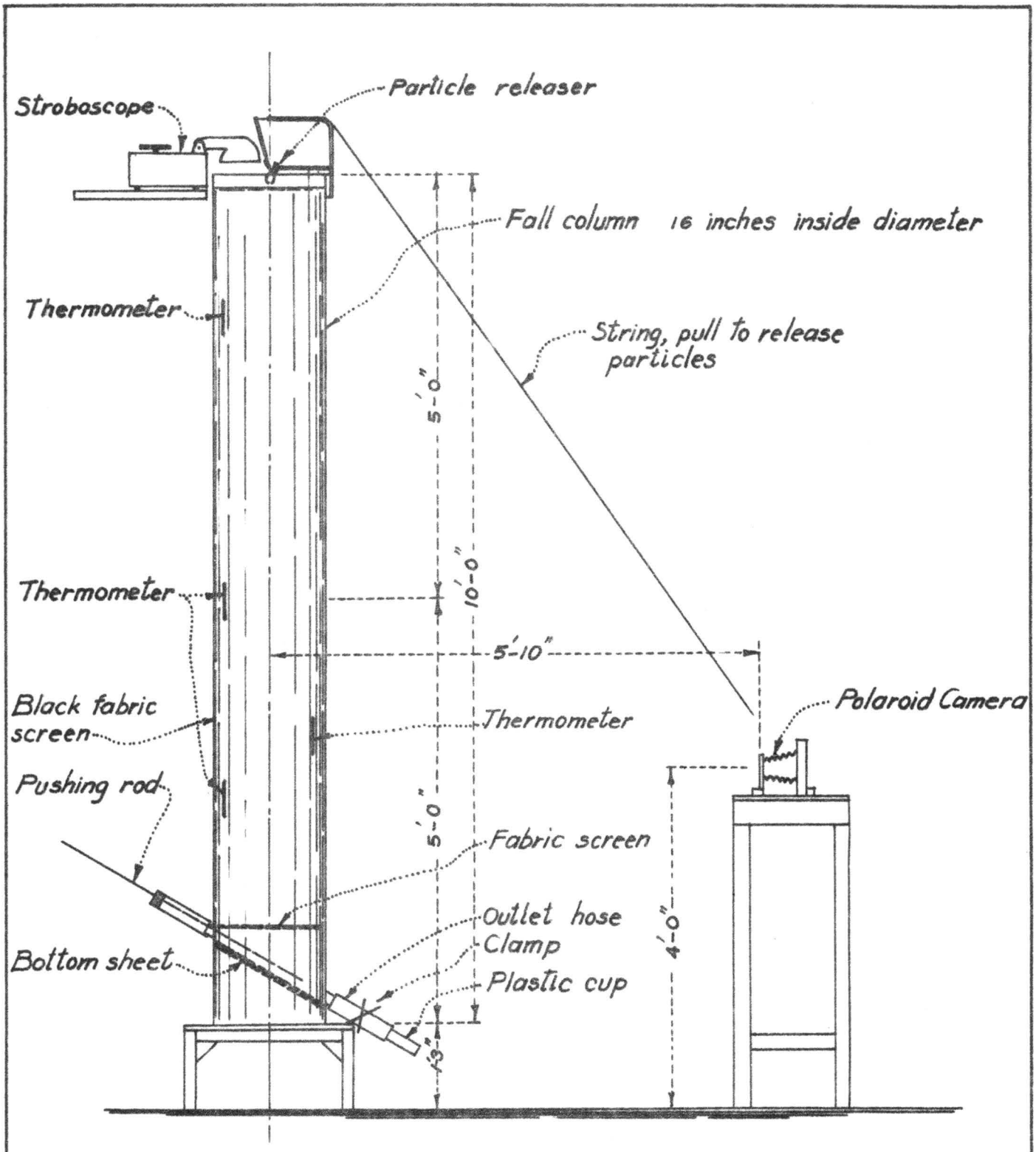

FIG. 7 - EQUIPMENT USED IN THE EXPERIMENT
(MIRROR NOT SHOWN)

of the column. This screen was used for catching the particles and then dropping them onto the bottom cushion. A second opening in the fall column was diametrically opposite from the outlet. A 1/8-inch brass rod could be maneuvered through a rubber stopper in this opening so that the particles could be pushed toward the outlet (see Fig. 7).

The temperature of the fluid in the fall column was measured by four thermometers. Three of them were located near the wall at various points shown in Fig. 7. Another one was attached to a nylon line and lowered into the fall column for measuring the temperature of the fluid at various locations during the experiment.

In order to obtain a good contrast in the picture of the particle falling in the column, a black background made of black fabric was attached to the inside wall of the column.

A mirror, 14 x 54 inches, was installed at a distance of about 10 inches to the left of the column. It was positioned to view the lower half of the fall column at 90° to the view obtained from the front view. By photographing both the front view and the side view of the column simultaneously, the position of the particle in relation to the longitudinal axis was found.

(b) Mechanical releaser

A small steel frame containing a steel jaw was attached to the top edge of the fall column. The jaw could be opened by pulling a nylon string led from the mechanical releaser. The string was long enough to be pulled from the floor.

(c) Stroboscope

The stroboscope employed in this experiment had the specifications as follows:

Flashing rate--110-25,000 flashes per minute in three ranges: 110-690, 670-4170, and 4,000-25,000. Speeds up to 250,000 rpm could be measured.

Accuracy--1 percent of dial reading after calibration on middle range.

Calibration--Could be calibrated against power line frequency by panel screwdriver adjustment.

Flash duration--Approximately 1, 3, and 6 microseconds for high, medium, and low-speed ranges, respectively (measured at 10 percent of maximum intensity).

Peak light intensity--0.21, 1.2, and 4.2 million candlepower minimum on high-, medium-, and low-speed ranges, respectively. For single flash, 7 million candlepower.

Reflector beam angle--10° at half-intensity points.

(d) Scale

A calibration scale was made by marking on a white-painted steel tape at five centimeter intervals. A weight of approximately 100 grams was attached at the lower end of the tape to keep the tape in a vertical position while suspended in the fall column to obtain a photograph.

(e) Camera and film

The Polaroid Land camera model 95B was used in this work. It had a "bulb" setting which was necessary for this operation. The film, Polaroid Type 47 having a speed of ASA 3200, which delivered 3-1/2 x 4-1/2 inch print, was employed because it is the fastest Polaroid film available at present. The very fast film was necessary in this case because the intensity of light from the stroboscope was small.

2. Arrangement of the equipment

The fall column was located near a corner, and its top could be easily reached from a platform. The mechanical releaser was attached to the top edge of the column such that the particle releasing-jaw was at the center of the column. The stroboscope was placed on a wooden shelf built in the wall near the top of the fall column (see Fig. 7).

The camera was placed on a sturdy wooden platform about four feet tall and the lens of the camera was approximately 4 feet above the ground level and about 5 feet 10 inches from the vertical centerline of the fall column. At such a location the camera was able to photograph the entire lower half of the column and the side view of the column in the reflection mirror at the left.

The end of the string from the mechanical releaser was placed near the camera so that it might be pulled to open the releaser jaw just before pressing the camera shutter.

A sketch and photograph showing the arrangement of the equipment are shown in Fig. 7 and Fig. 8 respectively.

3. Particles

The particles were composed of stainless bearing balls cemented together in two main types of arrangements. For Type I, the stainless balls were arranged to give the smallest possible porosity while for Type II, the balls were arranged to yield possible maximum voids (see Fig. 9).

The porosity of Type I and Type II were approximately .175 and .380, respectively. The porosity of the particles was defined by,

$$\text{Porosity} = \frac{\text{Pore volume}}{\text{Total volume of the particle}} .$$

The pore volume was obtained by subtracting the solid volume from the total volume of the particle.

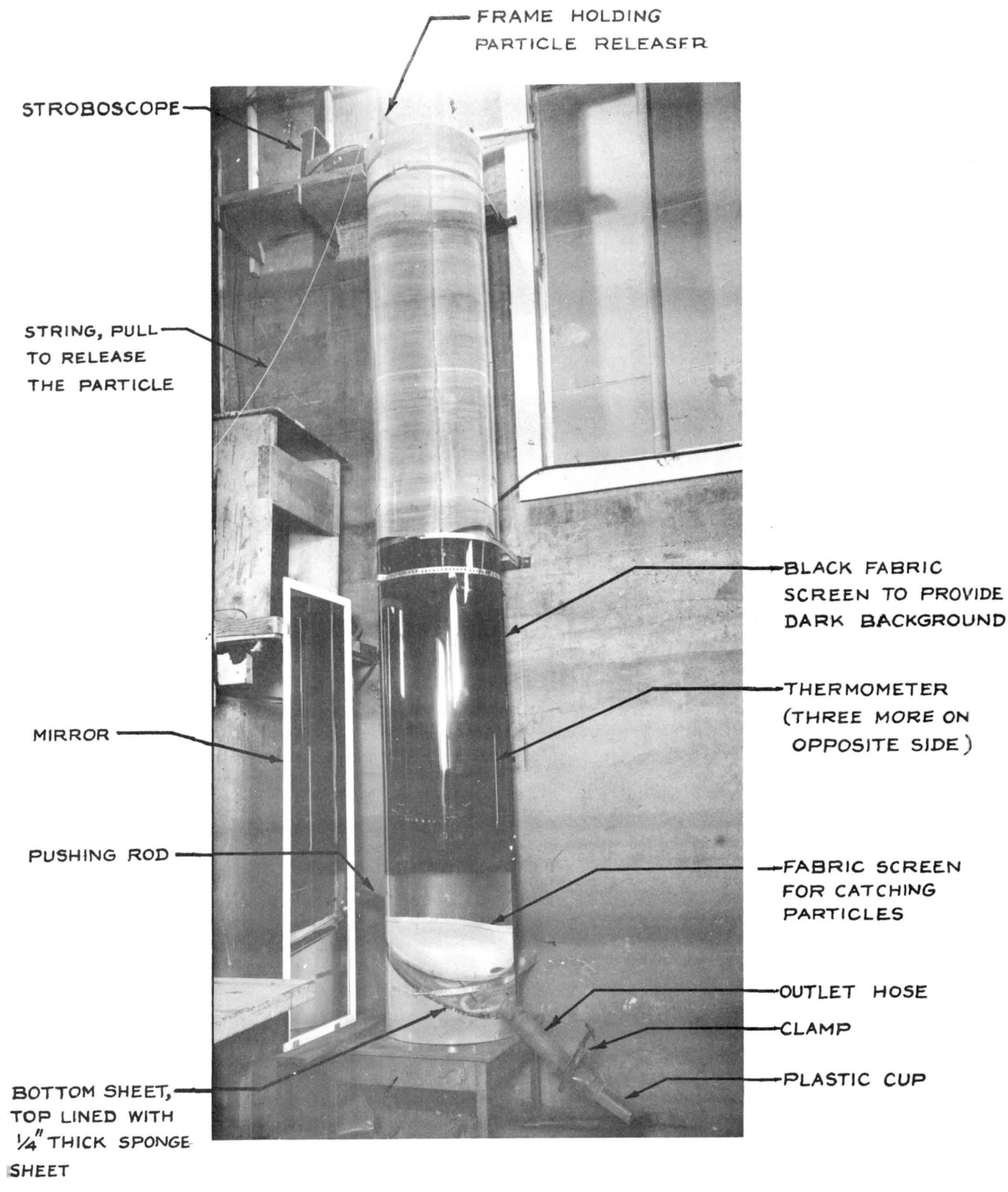

FIG. 8 - FALL COLUMN, 10 FEET LONG AND 16 INCHES IN DIAMETER

The total volume was the volume of the particle after all the pores were sealed as shown in Fig. 9.

The bearing balls employed in making the particles were of three sizes; 1/8 inch, 3/16 inch, and 1/4 inch in diameter. By using the same patterns of arrangement for each size of the bearing balls, three different sizes of particles were obtained for each type.

Thus, there were six particles which were porous. Three belong to Type I (i.e. the denser type) and the other three to Type II (i.e. the more porous particle) (Fig. 9).

Then, another set identical to the set described above was made. But, for this set, all the pores were sealed with plastic modelling clay and coated with a waterproof epoxy cement on the exterior surface. By doing so, no flow through the interior of the particles would exist while it was moving in the fluid. The particles of this type was designated as the "sealed type."

The total number of different particles used in this experiment was twelve; six of them were porous and another six were sealed. Each of the sealed particles was identical to a corresponding one of the porous type as far as the dimensions and bearing ball arrangement were concerned. They were different only in that one of them was sealed.

A nylon thread, about .001 inch in diameter and 1/2 inch in length was attached to each particle. This thread was used for suspending the particle from the jaw of the mechanical releaser. This was done to standardize the orientation of the particle at the instant of release.

The specific gravity of the particles was found by weighing them in air and in distilled water. The specific gravity was computed by the equation

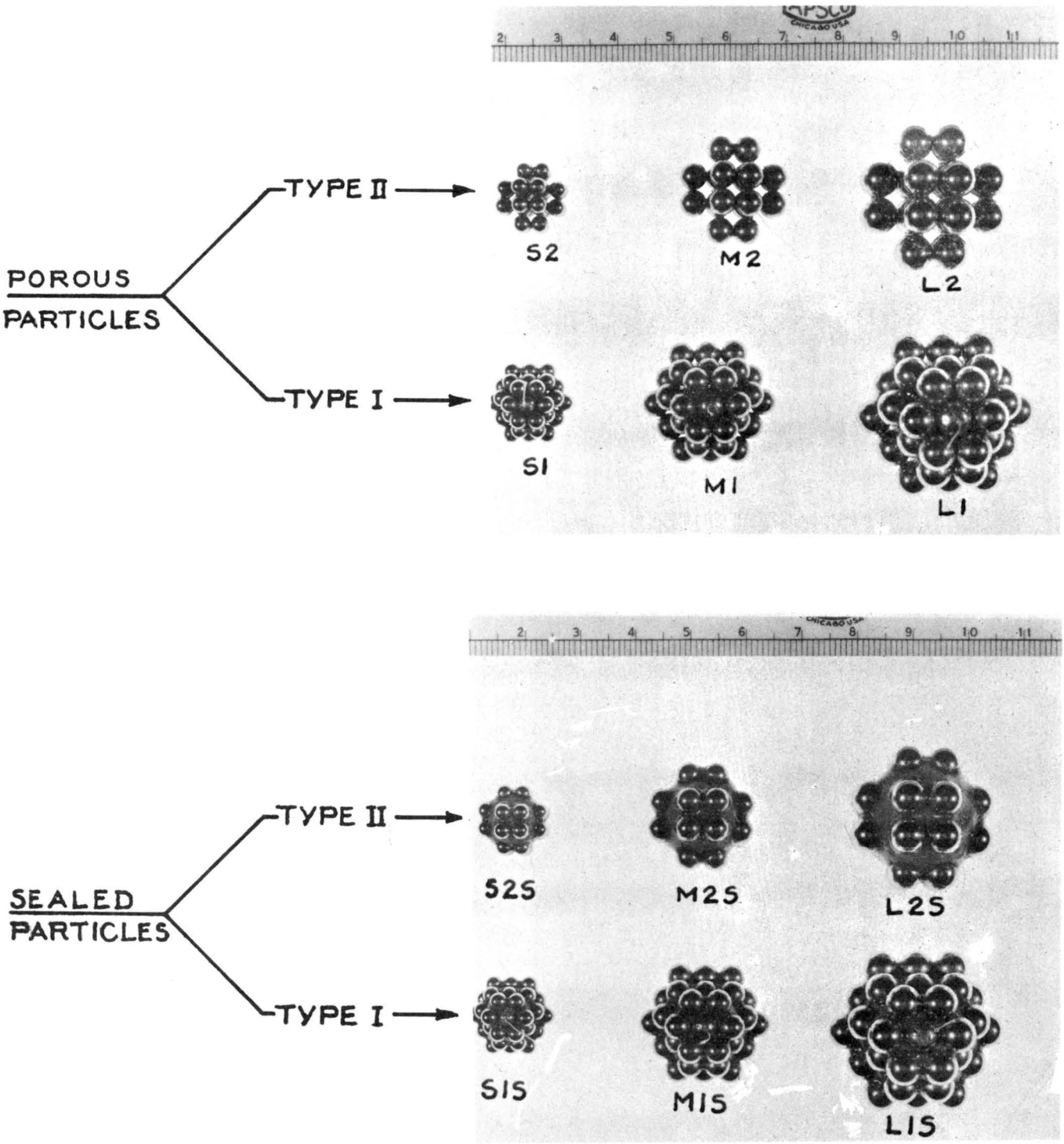

S = SMALL, M = MEDIUM, L = LARGE,

FIG. 9 - PARTICLES AND THEIR SYMBOLS

$$\text{Specific gravity} = \frac{\text{Weight of the particle in air, gms}}{\text{Weight of distilled water having volume} = \frac{4}{3}\pi d_n^3},$$

where d_n = nominal diameter, or the diameter of sphere having the same volume as the sealed particle. For porous particles, the nominal diameter was taken as equal to that of the sealed one of the identical size and bearing-ball arrangement.

For convenience, symbols were used for designation of the type and size of particles. See Fig. 9 for the particles and their symbols.

The nominal diameter of a sealed particle was defined as the diameter of a sphere having the same volume as the particle.

The nominal diameter and the specific gravity of the particles are tabulated in Table I.

4. Fluids

In order to obtain the drag coefficient of the particles at various values of Reynolds number, six fluids having six different viscosities, ranging from approximately .01 to 9 stokes, were used in the experiment.

The fluids were water (from the city water line), pure glycerine (synthetic grade), and four mixtures of water with glycerine. The proportion of mixtures and their corresponding designations are shown on the next page.

The viscosity of the fluids was determined with a Stormer viscosimeter. The curves showing the viscosity and the specific gravity of the fluids at various temperatures are in Figs. 10 and 11.

The water and glycerine were mixed by means of a centrifugal pump. The quantities of water and glycerine for the desired proportion

Symbol	Percent glycerine by volume	Percent water by volume	Approx. viscosity at 20°C stokes	Approx. specific gravity at 20°C
F1	0	100	.01	.998
F2	40	60	.04	1.114
F3	70	30	.29	1.197
F4	85	15	1.09	1.227
F4a	90	10	1.61	1.235
F5	100	0	9.42	1.253

were poured into the fall column. The outlet at the lower end of the fall column was connected to the pump inlet, and a hose was connected from the pump-outlet to the top of the fall column. The pump was then turned on and the fluid was circulated through the pump. The fluid was thus circulated for two or three hours to insure uniform mixing. The fluid was then left at rest for about two to three days to allow the air bubbles, which were formed as the result of the mixing, to rise before starting the experiment.

B. Procedure

The procedure employed in the experiment is described step by step as follows.

1. Preparation of fluids--The desired fluid was poured or mixed in the fall column. Then, it was left in the column until all the air bubbles disappeared and the fluid was very clear.

2. Preparation of particles--Each particle, before being dropped, was immersed in the same fluid heated to about 60° centigrade for approximately 10 minutes. The particle was then transferred into a dipper

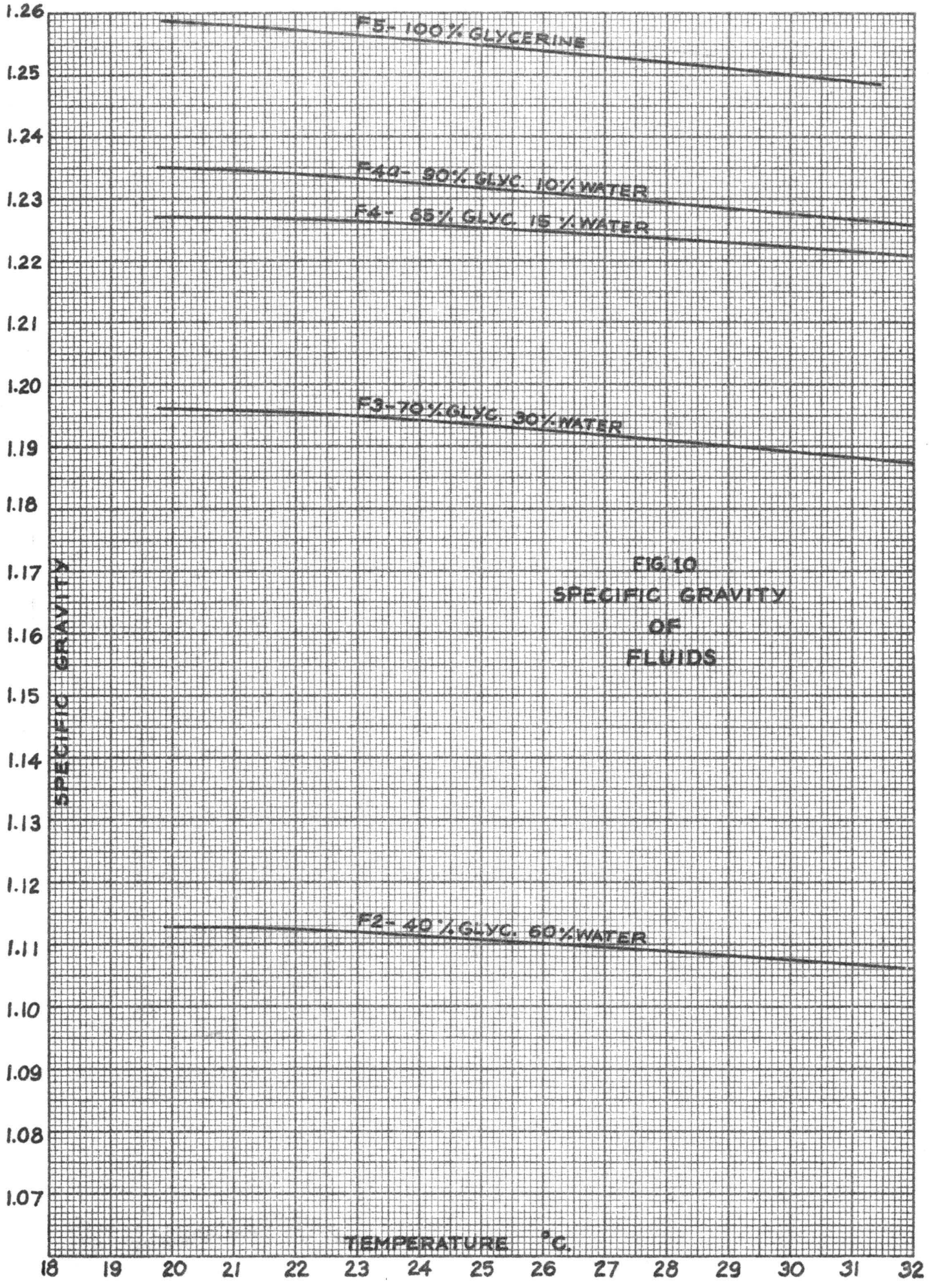

FIG. 10
SPECIFIC GRAVITY
OF
FLUIDS

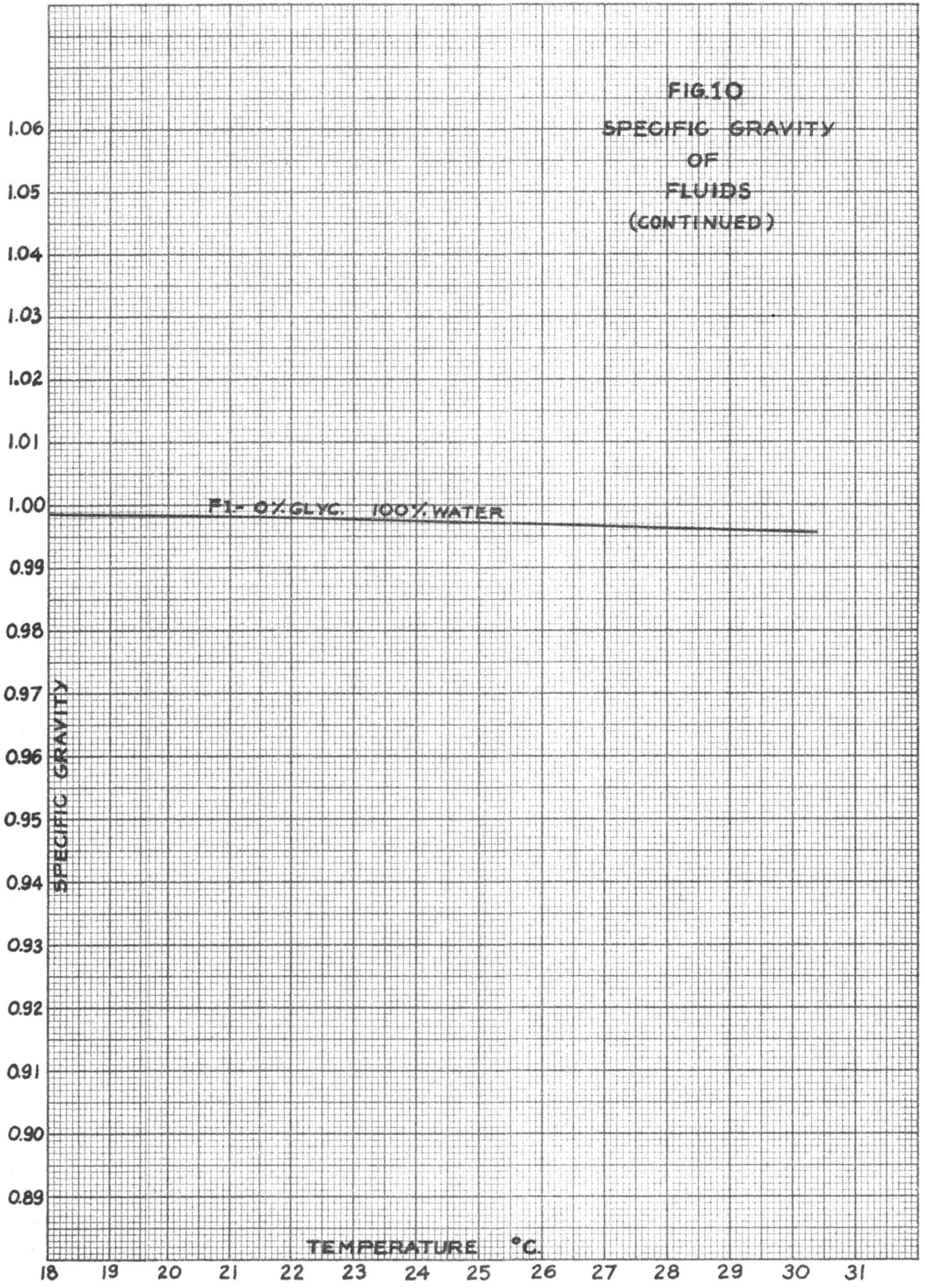
FIG.10
SPECIFIC GRAVITY
OF
FLUIDS
(CONTINUED)
F1- 0% GLYC. 100% WATER
SPECIFIC GRAVITY
1.06
1.05
1.04
1.03
1.02
1.01
1.00
0.99
0.98
0.97
0.96
0.95
0.94
0.93
0.92
0.91
0.90
0.89
TEMPERATURE °C.
18
19
20
21
22
23
24
25
26
27
28
29
30
31

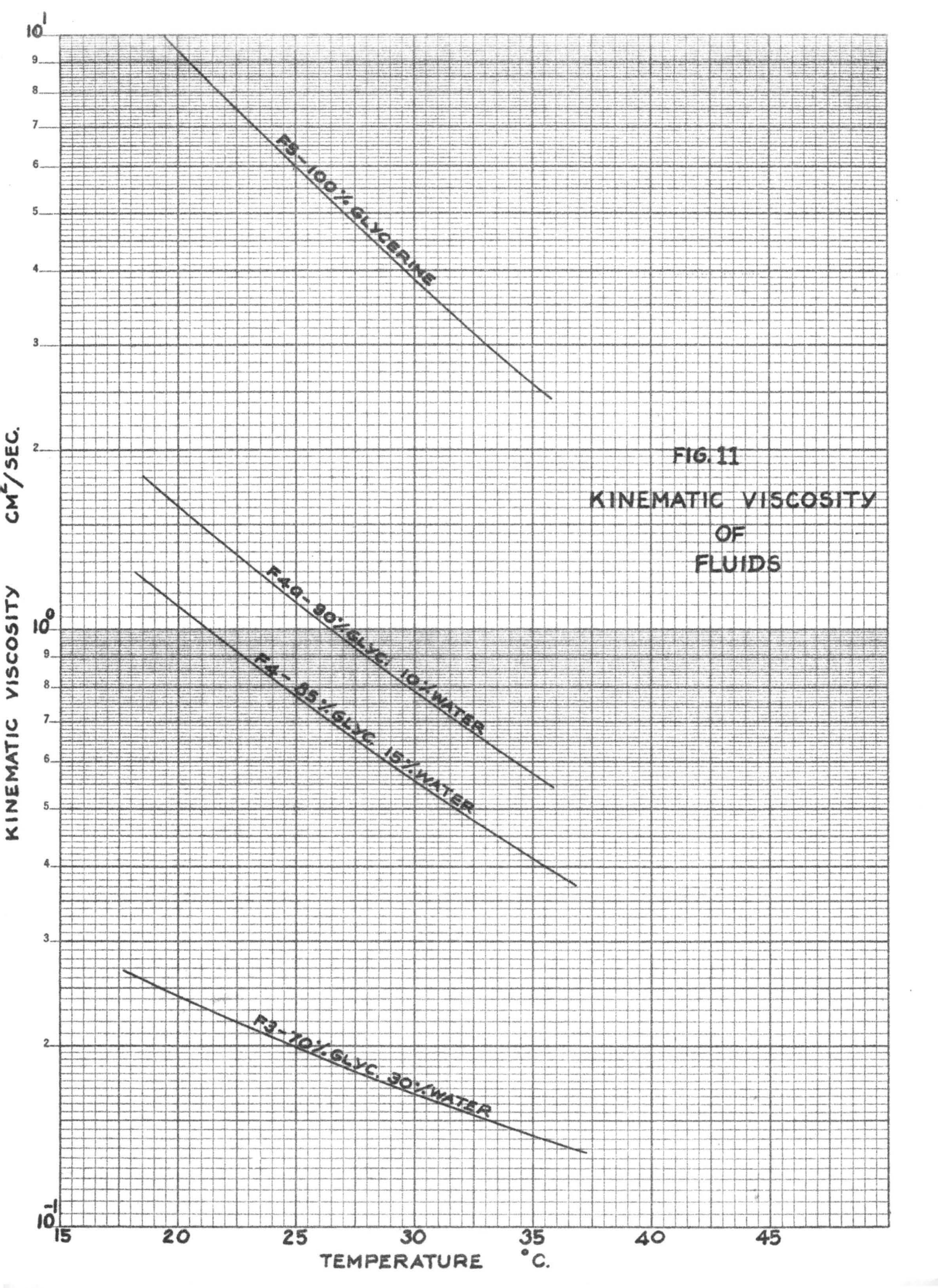
F5 - 100% GLYCERINE
F4-B - 90% GLYC. 10% WATER
F4 - 85% GLYC. 15% WATER
F3 - 70% GLYC. 30% WATER
FIG. 11
KINEMATIC VISCOSITY
OF
FLUIDS
KINEMATIC VISCOSITY CM²/SEC.
TEMPERATURE °C.
10¹
10⁰
10⁻¹
15
20
25
30
35
40
45

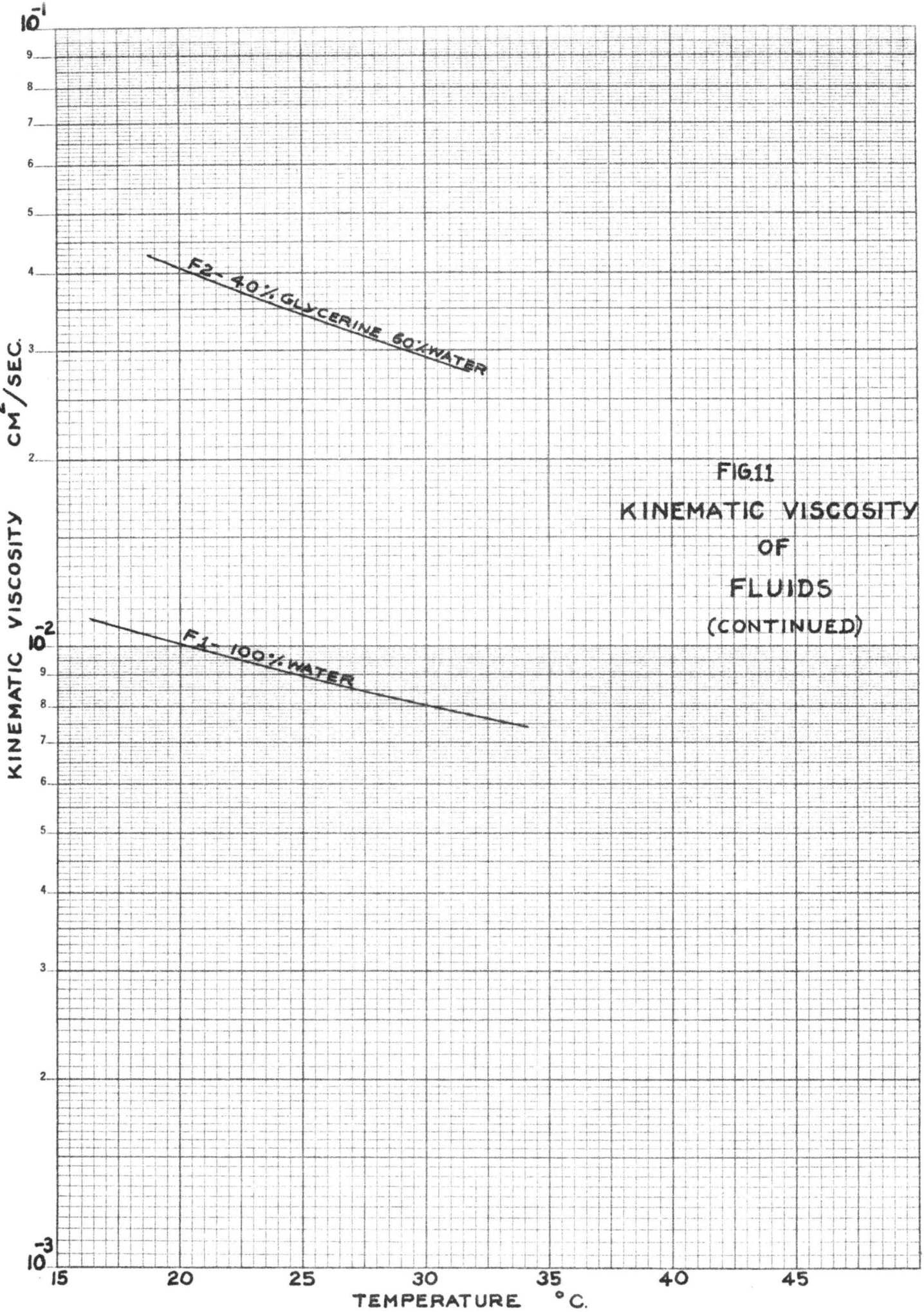

FIG.11
KINEMATIC VISCOSITY
OF
FLUIDS
(CONTINUED)

specially made so that the particle was submerged in the fluid all the time. By means of the dipper, the particle was transferred to the fall column and the nylon thread on the particle was inserted between jaws of the releaser. The particle was allowed to drop only after it had cooled down to the same temperature as the fluid in the column.

3. Setting of the stroboscope--It was desirable to limit the distance of descent between two consecutive images of the falling particle to about 1 centimeter (in the photograph). Therefore, the frequency on the stroboscope was set such that the actual fall distance during two consecutive flashes was approximately 10 centimeters. In this experiment, the frequency setting ranged from 150 to 700 revolutions per minute.

4. Setting of the camera--The shutter of the camera was set at "B" and the cable release was placed on one side of the camera. A lens opening of f8.8 was used throughout the entire experiment.

5. Operation--The stroboscope was turned on after all room lights were turned off. After the light began to flash, the string was pulled to open the jaw of the particle releaser. The shutter of the camera was pressed when the particle descended to the lower half of the column and it was released when the particle reached the bottom. The temperature was read from all four thermometers. The temperatures, the fluid mixture, the type of particle, and the frequency of the stroboscope were clearly marked on the photograph immediately after it was processed (the process to obtain the print took about 15 seconds after the camera shutter was released).

6. Scales--The steel calibration tape graduated at five centimeter intervals as mentioned previously was suspended at the center, at the left quarter point, the front quarter point, and the photographs of the

scale at the three locations were taken. A plastic scale overlay was then prepared from these photographs in the manner described in the second paragraph of this chapter.

7. Computation of fall velocity--Only the photographs of the particles falling within the middle half portion of the fall column were used in the experiment. All photographs of particles descending outside the middle half were discarded in order to avoid the influences of the wall on the particle velocity. Figure 12 shows some of the photographs actually used in the computation.

The fall velocity was obtained by applying eq. 4.1.

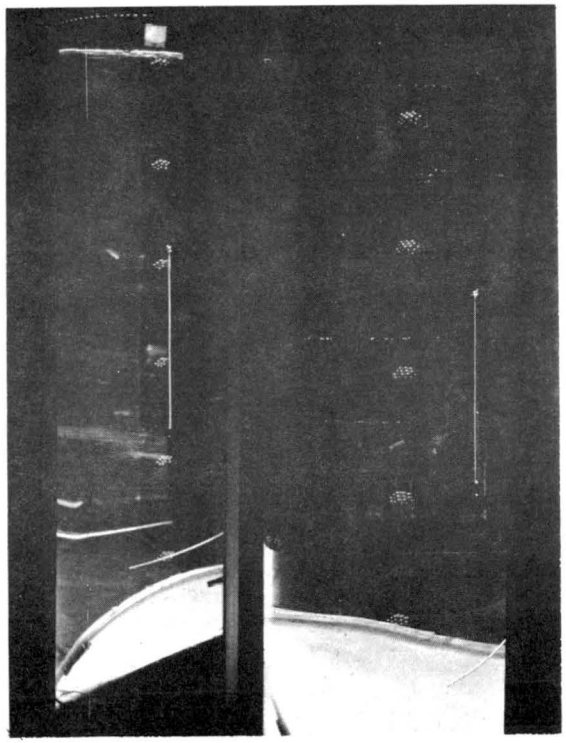

(A) PARTICLE L1 (LARGEST) DESCENDING IN GLYCERINE
STROBOSCOPE FREQUENCY 250 RPM.
TEMPERATURE 24.8° F

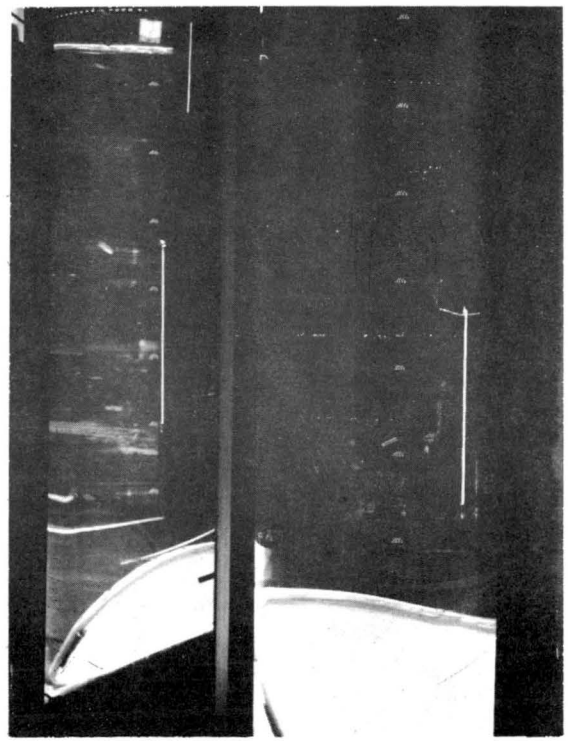

(B) PARTICLE S1 (SMALLEST OF TYPE I) DESCENDING IN GLYCERINE
STROBOSCOPE FREQUENCY 150 RPM.
TEMPERATURE 24.2° F

FIG. 12 - SAMPLES OF PHOTOGRAPHS USED IN THE COMPUTATION FOR THE TERMINAL FALL VELOCITY

CHAPTER V

DATA AND ANALYSIS

The data, complete with the computation for drag coefficient and Reynolds number, is tabulated and shown in Tables II to VIII, inclusive. The curves showing the relationship of the drag coefficient and Reynolds number for various types of particles are presented in Figs. 13 to 15.

The equations employed in the computation together with the detailed procedures of the computation will be presented in this chapter.

A. The Drag Coefficient

From eq. 3.7, the drag coefficient may be written as

$$C_D = 2 \frac{W_B}{A \rho_f V_o^2} .$$

1. For sealed particles--For the sealed particles $W_B = \frac{\pi d_n^3}{6}(\rho_s - \rho_f)g$, and $A = \frac{\pi d_n^2}{4}$,

where ρ_f = mass density of the fluid, in gm-sec^2/cm^4 ,

ρ_s = mass density of the particle, in gm-sec^2/cm^4 ,

d_n = nominal diameter of the particle (i.e. the diameter of a sphere having the same volume as the sealed particle. For porous particles, the nominal diameter was taken as equal to that of the sealed one of the identical size and bearing ball arrangement.

g = gravity acceleration (in this case $g = 980.7$ cm/sec^2).

By substituting W_B and A as above in eq. 3.7, the drag coefficient for the sealed particles may be expressed by

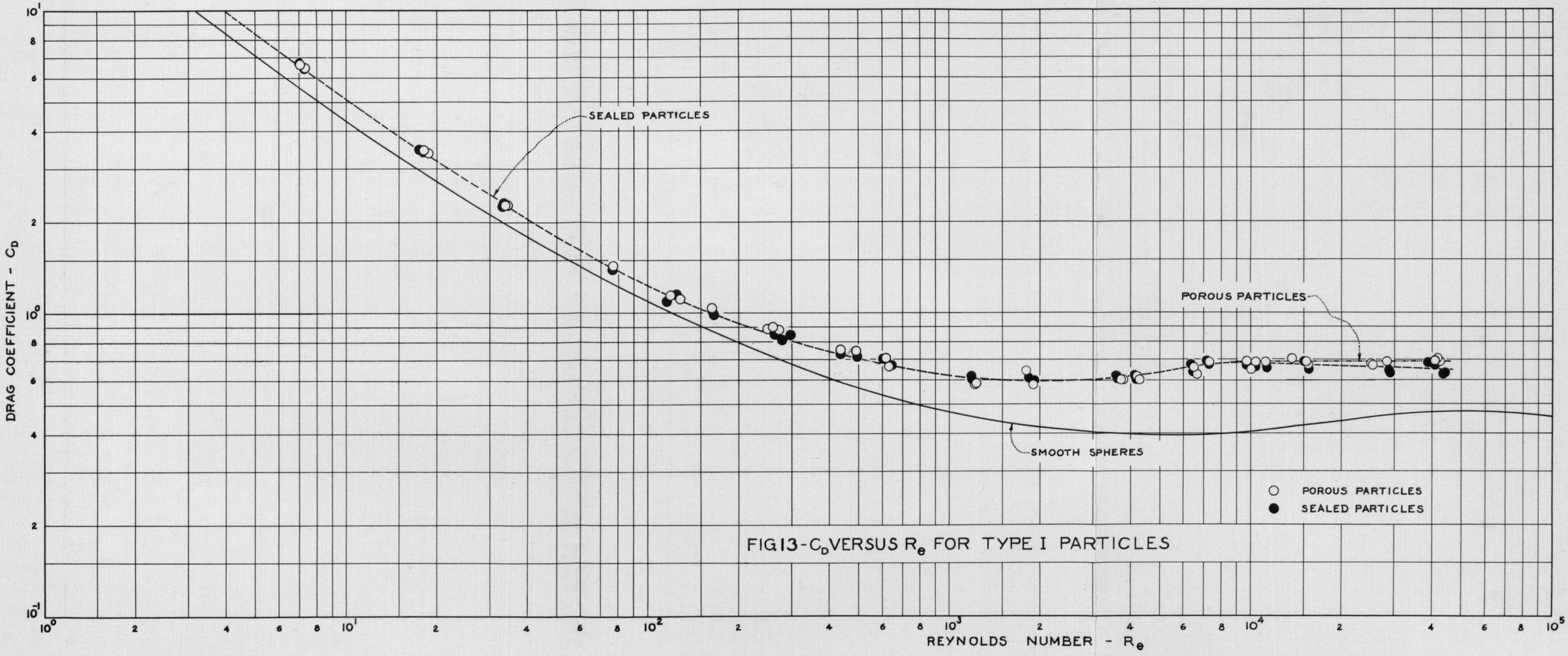

FIG 13 - C_D VERSUS R_e FOR TYPE I PARTICLES

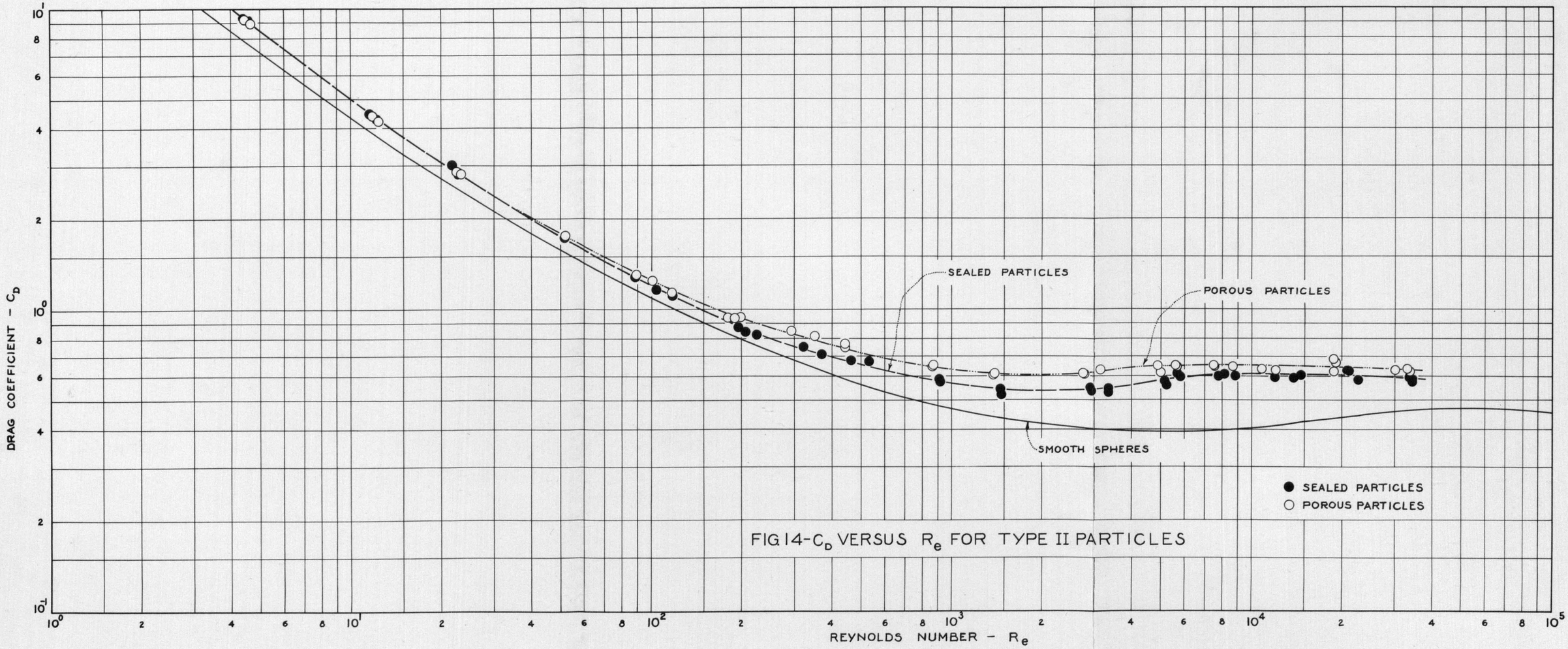

FIG 14-C_D VERSUS R_e FOR TYPE II PARTICLES

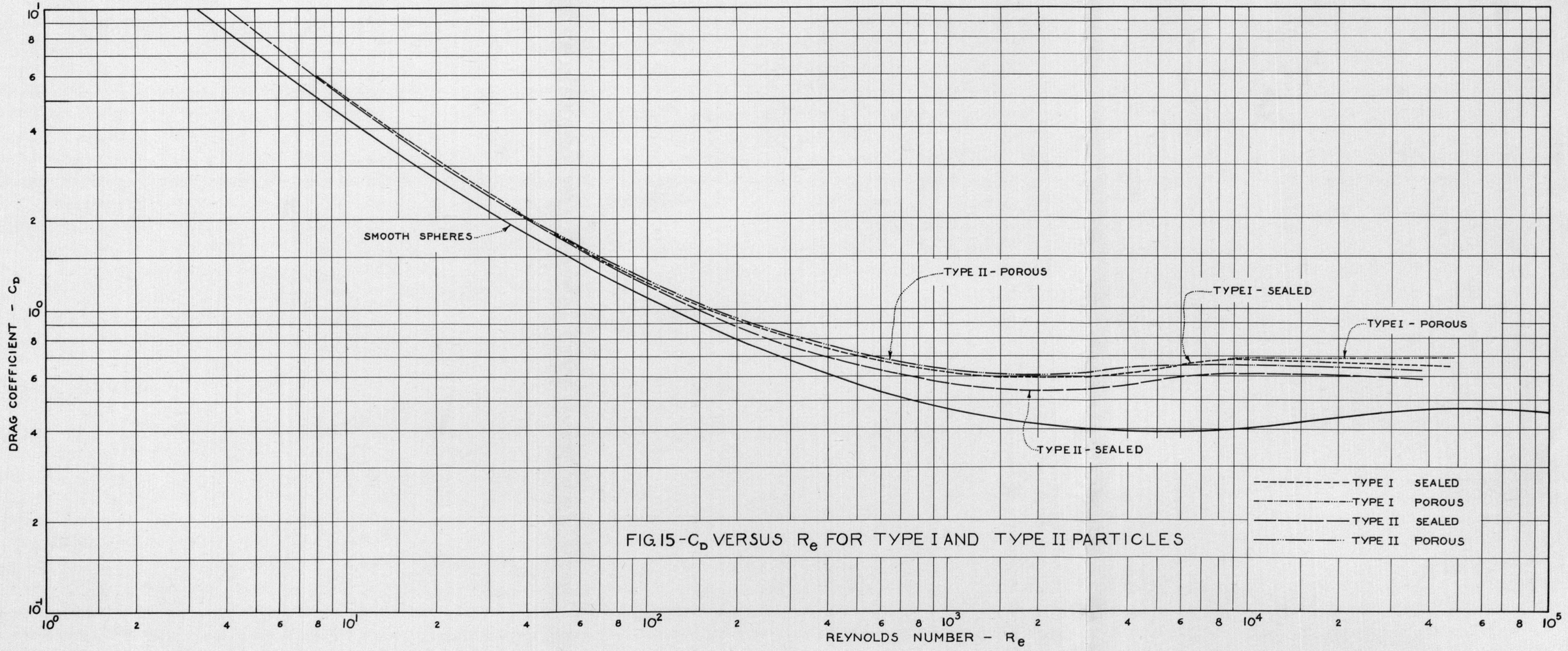

FIG. 15 - C_D VERSUS R_e FOR TYPE I AND TYPE II PARTICLES

$$C_D = \frac{4}{3} \frac{d_n (\rho_s - \rho_f) g}{\rho_f V_o^2} \qquad 5.1$$

Equation 5.1 was used for computing the value of the drag coefficient C_D for the sealed particles.

2. For porous particles--For the porous particles, A may be taken as $A = \frac{\pi d_n^2}{4}$, and $W_B = W_a - V_s \rho_f g$, 5.2

where W_a = weight in gms of the porous particle in air,

V_s = volume of the solid portion of the porous particle, in cc.

By substituting A and W_B from eq. 5.2, in eq. 3.7, the drag coefficient for the porous particles becomes

$$C_D = \frac{8}{\pi} \frac{W_a - V_s \rho_f g}{d_n^2 \rho_f V_o^2} \qquad 5.3$$

Equation 5.3 is employed for computing the value of C_D for the porous particles.

The specific gravity, the weight of the particles in air, the volume of the solid portion of the particle, and the nominal diameter of the particles are shown in Table I.

B. The Reynolds Number

The Reynolds number, Re, which indicates the relative effect of inertial and viscous forces, can be expressed as

$$Re = \frac{d_n V_o}{\nu} \qquad 5.3$$

where Re = Reynolds number, dimensionless,

d_n = nominal diameter of the particle, in cm,

ν = kinematic viscosity of the fluid, in cm^3/sec,

V_o = terminal fall velocity of the particle, in cm/sec.

C. C_D versus Re Curves

The curves showing the relationship of C_D and Re for the two types of particles, both sealed and porous, are drawn as shown in Figs. 13, 14, and 15.

Figure 13 shows the variation of C_D and Re of the sealed and porous particles of Type I. Similar curves for the particles of Type II are shown in Fig. 14. All the curves from both Figs. 13 and 14 were replotted and presented together in Fig. 15.

D. Drag Coefficient as Affected by the Porosity

The value of C_D as presented in Fig. 15 includes the effect of the roughness of the surface. Since the shape factor is approximately equal to unity and the general form of particles resembles a sphere, the drag coefficient of these particles, if their surfaces were smooth, should be the same as for the smooth sphere.

The effect of the surface roughness on the value of C_D at certain Reynolds numbers may be taken as the difference of the values of C_D, at the same Reynolds number, on the curve for the smooth sphere and the curve for the sealed particle used in the experiments.

The actual effect of the porosity on drag coefficient of the particles may be taken as the difference between the values of C_D of the porous particle and that of the corresponding sealed particle.

The curves of the variation of the drag coefficient of porous particles with respect to the Reynolds number shown in Fig. 16 were plotted by using the data as described in the preceding paragraph.

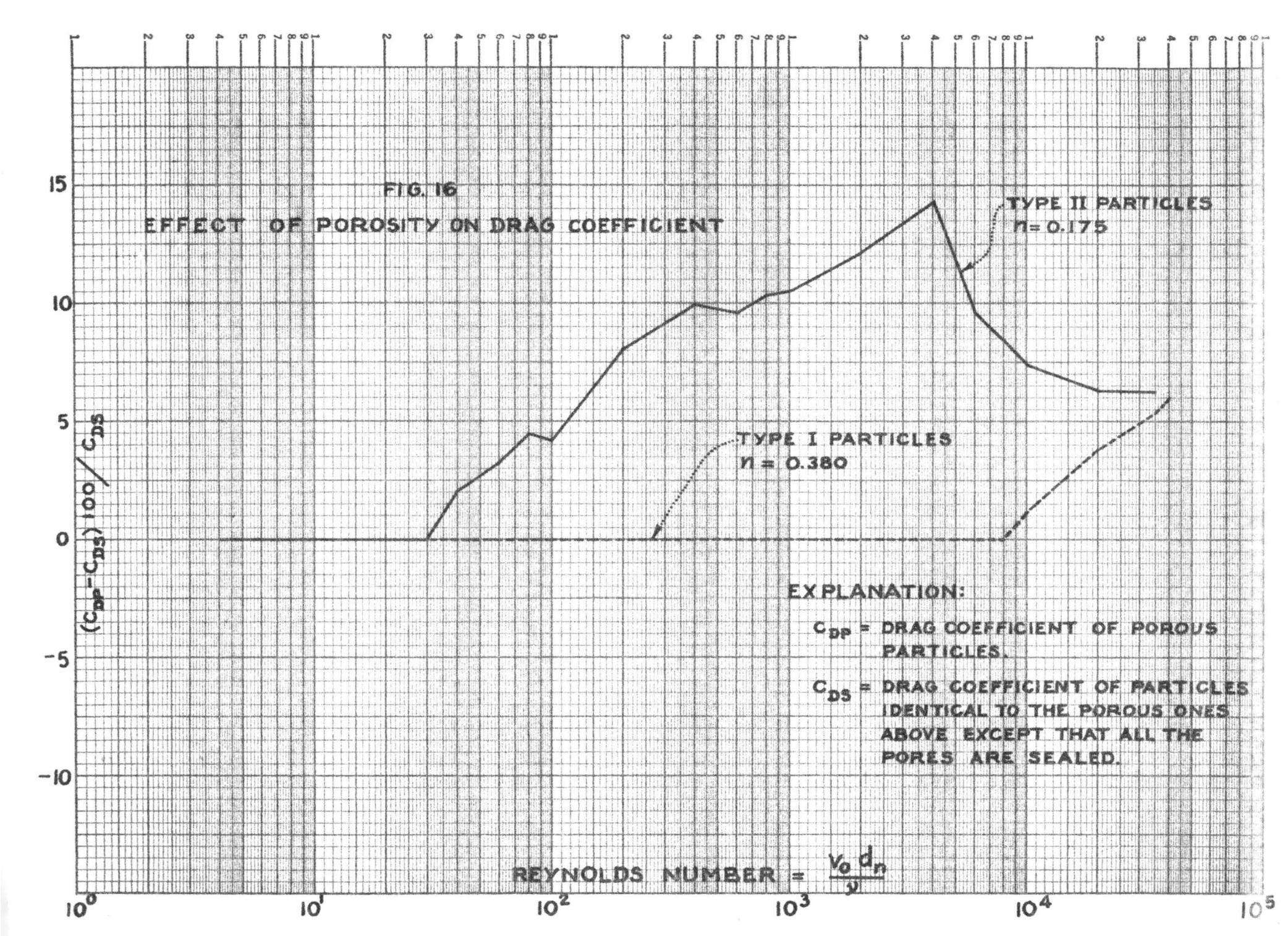
FIG. 16
EFFECT OF POROSITY ON DRAG COEFFICIENT
TYPE II PARTICLES
n = 0.175
TYPE I PARTICLES
n = 0.380
EXPLANATION:
C_{DP} = DRAG COEFFICIENT OF POROUS PARTICLES.
C_{DS} = DRAG COEFFICIENT OF PARTICLES IDENTICAL TO THE POROUS ONES ABOVE EXCEPT THAT ALL THE PORES ARE SEALED.
$(C_{DP} - C_{DS}) 100 / C_{DS}$
15
10
5
0
-5
-10
REYNOLDS NUMBER = $\frac{V_0 d_n}{\nu}$
10^0
10^1
10^2
10^3
10^4
10^5

CHAPTER VI

SUMMARY AND DISCUSSIONS

The drag coefficient of certain artificial porous particles has been found from experiments over a wide range of Reynolds number from approximately $Re = 5$ to $Re = 4.5 \times 10^4$. The drag coefficient of the corresponding particles with all the pores sealed has also been found experimentally. The resultant curves of C_D versus Re are presented in Figs. 13, 14 and 15 in Chapter V.

In this chapter a summary of the general characteristics of the motion of particles falling in various fluids is described and the results of the experiments are discussed.

A. General Observations

It may be observed from the photographs used for computing the fall velocity that for $Re < 10^3$ the particle appears to descend in a stable manner; the fall path is straight and there is negligible rotation of the particle.

At $Re > 10^3$, the path starts to deviate from a vertical straight line and the particle rotation becomes noticeable. However, the rotation is not so extensive that it should bear a significant influence on the drag coefficient.

It seems that for $Re > 10^4$ the orientation of the particle is more stable than for $10^3 < Re < 10^4$

B. Discussion of C_D versus Re Curves

1. All the C_D versus Re curves in Figs. 13 and 14 show high

values of C_D at low Re and C_D decreases as Re increases. This is in conformity with the theoretical analysis shown in eq. 3.8.

2. The curve for sealed particles is always above that for a smooth solid sphere throughout the entire range of Re . The greater values of C_D of the sealed particles may be caused by the surface roughness as will be explained by using eq. 3.6,

$$C_D = \frac{2\ (D_P + D_S + S)}{A\ \rho_f\ V_o^2} \quad .$$

At low Re , D_S predominates. Since D_S is proportional to the surface area, it is evident that the sealed particles, having larger surface area, will produce greater D_S than smooth spheres. In this case $S = 0$.

Since the roughness on the surface accelerates the formation of separation at a lower Re than when the surface is smooth, therefore, at the same Re , D_P of sealed (rough) particles will always be greater than D_P of smooth spheres.

From the preceding paragraphs and by using eq. 3.6, since sealed (rough) particles always have values of $(D_S + D_P)$ greater than that of smooth spheres, therefore C_D of sealed (rough) particles should be always higher than C_D of smooth spheres at the same Re.

3. It appears from the experiments that C_D of the sealed particles of Type I (i.e. denser type) is greater than C_D of the sealed particles of Type II (i.e. less dense type) at the same Re . This may be explained by using the same reasoning as in article B (2) above.

Type I sealed particles poses an external surface rougher than Type II sealed particles, therefore, at the same Re , $(D_S + D_P)$ of Type I

sealed particles will be greater than $(D_S + D_P)$ for the corresponding particles of Type II.

4. The experimental results show that for Type I particles, the C_D versus Re curves for porous and sealed particles coincide in the range of $4 < Re < 8 \times 10^3$. In other words, ΔC_D of the sealed and porous particles is very small. For Type II particles, ΔC_D begins at $Re = 30$ and show a significant deviation in values of C_D throughout the range of $Re > 30$.

In short, the C_D versus Re curves for both types conform to the theory presented in Chapter III that ΔC_D is small at low Re and it increases as Re increases.

5. The C_D versus Re curves show that the porous particles always have C_D higher or almost equal to C_D of the corresponding sealed ones.

(a) C_D of a porous particle will be almost equal to C_D of a corresponding sealed one when ΔC_D is sufficiently small, as in the range of low Re as described in Chapter III.

(b) C_D of a porous particle will be higher than C_D of a corresponding sealed one because W_B of the porous particle is greater than W_B of the corresponding sealed one. Equation 3.7 indicates that C_D of the porous particle will be higher than C_D of the corresponding sealed one.

6. The experimental results show greater values of ΔC_D for Type II particles than for Type I particles at the same Re (Figs. 13, 14, and 16). This may be explained by using eq. 3.7,

$$C_D = 2 \frac{W_B}{A \rho_f V_o^2} .$$

Let ΔC_D be the difference in values of C_D of a porous particle and a corresponding sealed particle at the same Re , ΔC_D may be written as

$$\Delta C_D = 2 \frac{\Delta W_B}{A \rho_f V_o^2} \qquad 6.1$$

where ΔW_B = difference in the bouyant weight of a porous particle and a corresponding sealed particle.

Type II particles, being more porous than Type I particles, will have greater ΔW_B than that of Type I. Therefore, from eq. 6.1, ΔC_D for Type II particles is larger than for Type I particles.

7. It should be emphasized here that the results presented in this report are for artificial particles constructed by cementing bearing balls together in a particular arrangement only. Particles having the same porosity may be built from bearing balls of the same or a different size and in the same or different arrangement. The same drag coefficient, however, would not necessarily be obtained.

C. Suggestion for Further Study

1. Since it is not possible to isolate the effect of the porosity alone on the drag coefficient presented in this report, an experiment employing porous particles having smooth surfaces should be attempted to find the influence of the porosity alone on drag coefficient.

2. Another experiment similar to the one presented in this report should be conducted by using particles having the same surface roughness and porosity as those used here, but differing in the arrangement.

3. The experiment should be extended to the range of higher Reynolds number and by using porous particles having porosity different from those used in this report. The results of this experiment should show

whether the reasoning presented herein about ΔC_D is consistent. Figure 17 shows a sketch of the curves obtained in this report and curves one might expect from the proposed experiment.

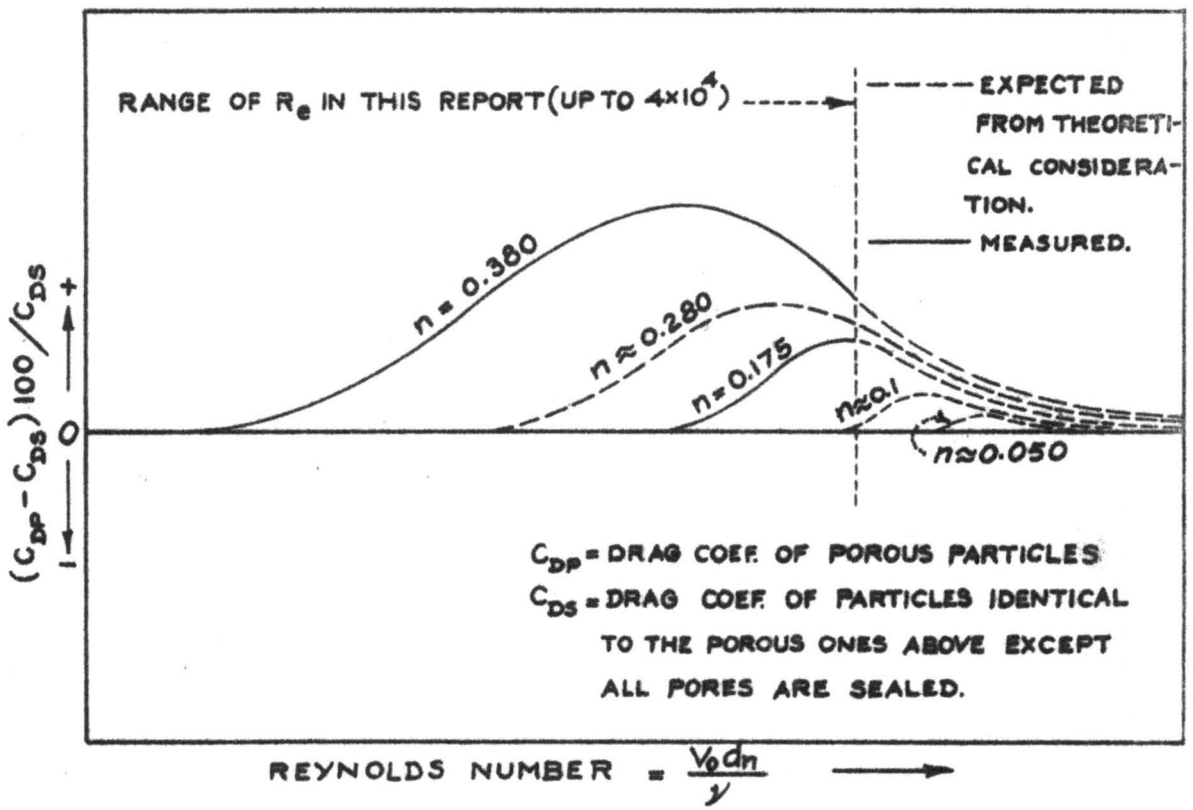

FIG. 17- C_D AS A FUNCTION OF R_e FOR PARTICLES OF VARIOUS POROSITIES.

BIBLIOGRAPHY

1. Albertson, M. L., Barton, J. R., and Simons, D. B. Fluid Mechanics for Engineers. Prentice-Hall, Inc. 1960. 567 p.

2. Goldstein, S., ed. Modern Developments in Fluid Mechanics. 2 volumes, London, Oxford University Press, 1938, 702 p.

3. Jenson, V. G. Viscous Flow Round Sphere at Low Reynolds Numbers (less than 40), Royal Society of London. Proceedings, Series A, 249(1258):346-366, January 13, 1959.

4. Kaufmann, Walther. Fluid Mechanics. McGraw-Hill Book Company, Inc. 1963, 432 p.

5. Lane, E. W. Hydraulic Engineering Aspects of Sediment Transportation and Deposition. Mimeograph, Lecture given at U.S. Bureau of Reclamation, Denver, 1946, 22 p.

6. McNown, J. S., Lee, H. M., McPherson, M. B., and Engez, S. M. Influence of Boundary Proximity on the Drag of Spheres. Seventh International Congress of Applied Mechanics. Proceedings, London, England, p. 17-19, September 1948.

7. McNown, J. S., and Malaika, Jamil. Effects of Particle Shape on Settling Velocity at Low Reynolds Numbers. American Geophysical Union. Transactions, 31:74-82:1950.

8. McNown, J. S. Particles in Slow Motion. LaHouille Blanche. 6(5):701-710, 718-722, September-October, 1951.

9. Prandtl, L. Mechanics of Viscous Fluids in Aerodynamic Theory. Vol. 3. Durand Reprinting Committee, Pasadena.

10. Rouse, Hunter. Fluid Mechanics for Hydraulic Engineers. Dover Publications Inc., New York. 1961 (unabridged and corrected republication of the 1938 edition) 422 p.

11. Schlichting, H. Boundary Layer Theory. McGraw-Hill Book Company, Inc. 1960. 647 p.

12. Schulz, E. F., Wilde, R. H., and Albertson, M. L. Influence of Shape on the Fall Velocity of Sedimentary Particles. Missouri River Division, Sedimentation Series. Report No. 5, Corps of Engineers, U.S. Army, Omaha, Nebraska, 1954. 161 p.

13. Sherman, Irving. Flocculent Structure of Sediment Suspended in Lake Mead. American Geophysical Union. Transactions, 34(3):395-406, June 1953.

BIBLIOGRAPHY--Continued

14. Some Fundamentals of Particle Size Analysis. Study of Methods Used in Measurement and Analysis of Sediment Loads in Streams. St. Anthony Falls Hydraulic Laboratory, Minneapolis, Minnesota, December 1957. 55 p. Report No. 12.

15. Wilson, D. H. Hydrodynamics. Edward Arnold (Publishers) Ltd. 1959. 149 p.

APPENDIX

TABLE I

PHYSICAL PROPERTIES OF PARTICLES

Particles	Weight in air gm.	Volume of solid cc.	Specific Gravity	Nominal Diameter cm.
S1	7.655	0.96	6.55	2.605
S2	4.296	0.54	4.94	2.360
M1	25.569	3.23	6.53	1.957
M2	14.343	1.82	4.89	1.777
L1	60.457	7.64	6.54	1.308
L2	33.944	4.28	4.89	1.188
S1S	7.750	1.17	6.64	2.605
S2S	4.630	0.88	5.24	2.360
M1S	25.978	3.92	6.64	1.957
M2S	15.406	2.94	5.25	1.777
L1S	61.312	9.23	6.62	1.308
L2S	36.005	6.87	5.26	1.188

TABLE II - SERIES F1

PARTICLES IN WATER

Picture No.	Particle	Terminal fall velocity V_o cm/sec	C_D	Re
31	L1	168.2	.692	40,800
34	L1	167.0	.701	41,630
39	L1	168.9	.686	42,600
15	L2	145.3	.627	30,080
38	L2	144.4	.636	33,120
76	L2	146.0	.622	33,260
26	M1	149.3	.668	25,500
28	M1	148.5	.675	25,470
35	M1	147.9	.683	28,420
13	M2	120.2	.685	18,840
23	M2	122.0	.668	19,140
20	S1	118.0	.703	13,720
36	S1	119.5	.684	15,420
40	S1	120.6	.673	15,540
21	S2	102.5	.636	10,800
37	S2	103.0	.630	12,080
68	L1S	174.0	.632	44,000
75	L1S	174.8	.627	43,700
53	L1S	169.2	.668	41,100
47	L1S	167.6	.681	38,800
64	L2S	149.4	.587	34,300
74	L2S	150.6	.582	34,420
67	L2S	148.5	.594	33,900
63	M1S	149.8	.643	28,800
69	M1S	151.0	.632	29,050
50	M2S	126.3	.623	21,160
55	M2S	130.1	.587	22,680
65	M2S	126.0	.626	21,120

TABLE II - SERIES F1--Continued

Picture No.	Particle	Terminal fall velocity V_o cm/sec	C_D	Re
61	S1S	117.8	.692	15,200
73	S1S	122.3	.644	15,610
57	S2S	106.0	.593	11,960
60	S2S	106.3	.592	13,820
66	S2S	104.8	.506	14,600

TABLE III - SERIES F2--FIRST RUN
PARTICLES IN MIXTURE OF 40% GLYCERINE
AND 60% WATER
(By volume)

Picture No.	Particle	Terminal fall velocity V_o cm/sec	C_D	Re
193	L1	163.0	.647	10,050
203	L1	157.5	.690	9,730
215	L1	158.7	.683	10,430
185	L2	134.0	.653	7,500
198	L2	134.6	.648	7,530
192	M1	143.5	.625	6,660
205	M1	140.0	.658	6,500
187	M2	119.0	.617	5,010
197	M2	116.2	.649	4,890
188	S1	124.0	.559	3,860
194	S1	120.5	.599	3,742
217	S1	120.6	.599	3,745
191	S2	97.8	.612	2,755
207	S2	98.2	.607	2,770
218	S2	98.2	.607	2,770
202	L1S	157.5	.669	9,720
213	L1S	158.4	.660	10,440
201	L2S	138.5	.595	7,760
216	L2S	137.3	.606	8,200
204	M1S	137.4	.671	6,380
212	M1S	141.0	.638	6,540
200	M2S	123.8	.560	5,230
211	M2S	122.3	.575	5,160
189	S1S	118.3	.602	3,670
209	S1S	117.3	.612	3,640
195	S2S	103.8	.537	2,930
208	S2S	103.3	.549	2,900

TABLE IV - SERIES F2--SECOND RUN

PARTICLES IN MIXTURE OF 40% GLYCERINE

AND 60% WATER

(By volume)

Picture No.	Particle	Terminal fall velocity V_o cm/sec	C_D	Re
225	L1	158.3	.684	11,200
228	L2	135.2	.644	8,670
224	M1	137.3	.684	7,310
239	M2	116.0	.653	5,590
241	M2	116.8	.644	5,630
236	S1	118.7	.615	4,210
226	S1	120.4	.598	4,290
227	S2	97.3	.631	3,150
242	S2	97.0	.633	3,126
234	L1S	160.5	.657	11,360
231	L2S	137.7	.600	8,850
238	M1S	132.2	.725	9,620
230	M1S	137.0	.676	7,290
235	M1S	135.8	.691	7,130
229	M2S	120.8	.593	5,820
234	M2S	119.0	.610	5,680
237	S1S	117.0	.620	4,160
232	S1S	118.8	.600	4,220
233	S2S	103.2	.545	3,335
236	S2S	105.1	.526	3,350

TABLE V - SERIES F3

PARTICLES IN MIXTURE OF 70% GLYCERINE AND 30% WATER

(By volume)

Picture No.	Particle	Terminal fall velocity V_o cm/sec	C_D	Re
156	L1	165.5	.578	1,908
170	L1	157.3	.641	1,805
158	L2	132.9	.612	1,393
169	L2	133.8	.604	1,390
157	M1	143.5	.577	1,220
167	M1	142.6	.585	1,227
159	M2	111.0	.654	873
165	M2	110.9	.655	868
161	S1	106.3	.706	619
166	S1	109.7	.661	632
160	S2	83.9	.767	446
168	S2	85.3	.744	447
171	L1S	160.3	.603	1,840
179	L1S	161.0	.598	1,914
162	L2S	138.7	.542	1,454
176	L2S	141.5	.519	1,470
163	M1S	137.3	.618	1,190
175	M1S	137.7	.616	1,185
164	M2S	116.9	.575	922
174	M2S	116.1	.584	917
172	S1S	104.7	.706	604
177	S1S	107.4	.672	642
173	S2S	88.5	.675	464
178	S2S	89.2	.666	533

TABLE VI - SERIES F4

PARTICLES IN MIXTURE OF 85% GLYCERINE

AND 15% WATER

(By volume)

Picture No.	Particle	Terminal fall velocity V_o cm/sec	C_D	Re
108	L1	143.4	.746	492.
118	L1	143.0	.753	438.
107	L2	113.6	.814	352.
128	L2	115.5	.843	294.
135	M1	114.2	.882	250.
141	M1	113.2	.898	261.
115	M2	91.5	.934	191.
126	M2	91.3	.937	181.
117	S1	83.6	1.107	128.5
129	S1	82.0	1.147	119.5
104	S2	64.8	1.248	101.5
119	S2	63.6	1.299	89.0
114	L1S	144.8	.716	496.
125	L1S	143.3	.729	439.
120	L2S	116.0	.750	322.
109	L2S	119.5	.707	371.
110	M1S	115.8	.841	298.
122	M1S	115.4	.847	265.
123	M2S	93.8	.868	196.
111	M2S	96.0	.828	225.
113	S1S	85.2	1.039	163.7
121	S1S	80.8	1.150	125.
140	S1S	83.0	1.093	116.
112	S2S	66.5	1.153	104.
124	S2S	63.2	1.279	88.4

TABLE VII - SERIES F4a

PARTICLES IN MIXTURE OF 90% GLYCERINE

AND 10% WATER

(By volume)

Picture No.	Particle	Terminal fall velocity V_o cm/sec	C_D	Re
142	L1	131.8	.877	274.7
146	L2	105.2	.943	199.0
145	M1	104.8	1.038	164.3
147	M2	82.2	1.131	116.8
143	S1	73.2	1.437	76.7
144	S2	54.6	1.752	52.0
148	L1S	134.3	.813	280.0
153	L2S	109.3	.840	206.7
149	M1S	105.8	.986	165.8
152	M2S	82.7	1.104	117.6
150	S1S	72.8	1.388	76.3
151	S2S	54.1	1.732	51.5

TABLE VIII - SERIES F5

PARTICLES IN GLYCERINE (SYNTHETIC GRADE)

Picture No.	Particle	Terminal fall velocity V_o cm/sec	C_D	Re
90	L1	81.40	2.256	33.80
81	L1	81.40	2.256	34.00
88	L2	60.00	2.862	22.50
79	L2	60.60	2.805	23.40
82	M1	57.75	3.447	18.10
97	M1	58.30	3.373	18.85
80	M2	42.70	4.206	12.42
89	M2	41.80	4.377	11.80
91	S1	33.80	6.600	7.05
98	S1	34.25	6.431	7.38
92	S2	23.60	9.170	4.46
99	S2	23.96	8.898	4.69
85	L1S	80.40	2.267	33.60
93	L1S	80.90	2.255	33.60
84	L2S	57.40	3.007	21.70
100	L2S	59.00	2.834	22.90
96	M1S	56.90	3.470	17.77
83	M1S	57.00	3.462	17.85
86	M2S	40.76	4.478	11.51
103	M2S	41.80	4.260	12.18
95	S1S	33.30	6.625	6.96
102	S1S	34.10	6.335	7.37
94	S2S	23.27	9.230	4.41
101	S2S	23.60	8.950	4.62